On Gravitational Binding Energy Evaluation

Nicolas Poupart[1*]

[1]Independent Researcher, Quebec, Canada.

Corresponding author(s). E-mail(s): nicolas.poupart@yahoo.fr;

The objective of this work is to calculate the total energy that would be released if all the stars of a galaxy underwent an idealized perfectly inelastic aggregation, while accounting exclusively for gravitational energy. This quantity represents the gravitational energy stored in the internal organization of the galaxy and potentially available for release. Through mass–energy equivalence, it implies a corresponding contribution to spacetime curvature that may account for the gravitational effects commonly attributed to dark matter.

The same binding-energy equation is derived through two distinct constructions. The first is entirely Newtonian and is established over nearly forty orders of magnitude in mass. The second combines external Newtonian gravitational work with relativistic black-hole absorption and extends the same mathematical structure to galactic scales.

The resulting equation is then confronted with galactic observations. Its predicted $M^{5/3}$ dependence is recovered empirically, while the coefficients governing the hierarchical contributions are independently constrained by photometric observations and remain close to the theoretically expected domain.

The method also projects galaxies into a stellar-population space derived from dynamics alone. The resulting populations correspond with independent GALEX and SDSS photometry, indicating that the reconstruction captures physical information about stellar content rather than merely reproducing the mass discrepancy.

These results support gravitational binding energy as a viable explanation for the dark mass inferred in galaxies. We finally examine the cosmological consequences of this interpretation and propose a gravitational–vacuum energy exchange as a possible resolution of the tensions arising at earlier cosmic epochs.

1 Introduction

The origin of the dark mass component inferred from galactic dynamics remains one of the central open questions in astrophysics [7]. Its presence is robustly established through multiple independent observations, including rotation curves and dynamical modeling [23, 24], as well as gravitational lensing measurements [1, 6]. However, its physical nature remains unknown.

At the same time, gravitational theory, both Newtonian and relativistic, has demonstrated remarkable accuracy across a wide range of scales. This raises the possibility that the observed discrepancy can be accounted for without invoking exotic matter or modified gravity, but by recognizing that gravitational potential energy is not straightforward to define and evaluate as an intrinsic contribution to the effective mass budget of astrophysical systems.

In standard formulations, gravitational potential energy is defined relative to an arbitrary reference level, typically taken at infinity. As a result, the expression $E = -GmM/d$ is well suited for describing reversible orbital dynamics, but it does not directly provide an intrinsic energy associated with the formation or internal organization of an extended many-body system.

More generally, the notion of potential energy becomes ambiguous when applied to complex self-gravitating systems. It quantifies the work required to separate constituents to infinity, rather than the energy associated with assembling matter into a bound configuration. Related ambiguities have long been recognized in classical mass renormalization [4] and in geometrical definitions of mass in general relativity [13, 15, 21].

A useful analogy is provided by nuclear binding energy. The mass of a helium nucleus is smaller than the combined mass of the hydrogen nuclei from which it may be formed, and this mass deficit is entirely accounted for by the energy released during the corresponding fusion process. The binding energy can therefore be determined by comparing two configurations containing the same conserved constituents, with one configuration initially dispersed and the other more tightly bound.

The primary objective of this work is to apply the same accounting principle to the gravitational organization of a galaxy. We calculate the gravitational energy that would be released if all its stars underwent a hypothetical perfectly inelastic aggregation into a single compact body, while accounting exclusively for gravitational energy. We investigate whether the mass equivalent of this released energy can entirely account for the dark mass inferred from galactic dynamics, just as the energy released during nuclear fusion accounts for the mass deficit of the resulting nucleus.

We define gravitational binding energy as the energy released when a distributed configuration is transformed into a maximally compact reference configuration while conserving total mass and constituent volumes. The corresponding volume-conserving sphere may be viewed as a configuration in which all constituents are placed side by side without altering their internal structure. It therefore introduces no additional compression of the constituents and provides a well-defined reference state for evaluating the gravitational energy released by their hypothetical perfectly inelastic aggregation.

The theoretical development proceeds in two complementary directions. We first derive the binding-energy equation entirely within Newtonian gravity and examine the conditions under which this construction can be extended from ordinary gravitational systems to the galactic scale. The limits of the compact volume-conserving interpretation are then considered explicitly, together with the continuation of the same energy accounting when aggregation leads to black-hole formation.

We then obtain the same functional form through an independent construction compatible with general relativity. The two derivations start from different physical descriptions but converge toward the same gravitational-energy equation. This agreement provides a central consistency test of the proposed evaluation before it is confronted with galactic observations.

The theoretical predictions are then subjected to a sequence of observational tests. The first concerns the mass scaling itself. The binding-energy construction predicts an intrinsic dependence proportional to $M^{5/3}$. When the exponent governing the galactic relation is allowed to vary so that the galaxies are projected within the theoretically admissible stellar-population bounds, the preferred values converge toward 5/3, in agreement with the predicted exponent.

A second test concerns the structure of the energy equation. The relative weights of its principal contributions are allowed to vary independently, and each resulting estimator is evaluated through the agreement between the predicted and observed GALEX and SDSS colors. The highest photometric scores are obtained for coefficients close to those expected from the theoretical constructions. The photometric optimum therefore falls within the region expected from the theoretical construction, although the global coefficient remains less sharply constrained, with the best solutions extending approximately over $\beta \simeq 0.5$–3.

The strongest test concerns the physical meaning of the reconstruction itself. The energy equation associates each galaxy with a position in stellar-population space. If this projection were only a numerical consequence of the fitting procedure, there would be no reason for the assigned populations to correspond to independent properties of the galaxies. We therefore test whether the projected galaxies retain a real connection with stellar population observables. The resulting correspondence provides an independent test of whether the populations inferred from the gravitational calculation represent physical properties of the galaxies rather than merely mathematical solutions of the energy equation.

Finally, we examine the cosmological consequences of this interpretation. Extending the gravitational-energy calculation to earlier cosmic epochs reveals potential tensions associated with the evolution of stellar populations and gravitationally bound structures. We show that these difficulties can be addressed through a simple extension in which gravitational and vacuum energy are allowed to exchange while their combined energy–momentum remains conserved. This provides a possible connection between the galactic dark-mass result, the cosmological dark sector, and a global thermodynamic description of the Universe.

1.1 Useful gravitational potential energy

If we consider the Newtonian gravitational force equation, $F = GmM/d^2$, integration from d to infinity gives the usual potential-energy expression $E_p = -GmM/d$. This expression is well suited to describing orbital dynamics, but its absolute value depends on the arbitrary choice of the zero of gravitational potential. For the purpose considered here, the physically relevant quantity is therefore the energy difference between two specified configurations of the same system.

For example, moving a mass m from a distance d to $d + h$ from a mass M gives:

$$\Delta E_p = E_p(d+h) - E_p(d) = \frac{GmMh}{d^2 + dh} \tag{1}$$

This energy difference is invariant under an additive transformation of the Newtonian potential and is therefore independent of the arbitrary choice of potential zero.

We now generalize this construction to two classical macroscopic bodies. The Newtonian formulation is first considered over an intentionally broad domain extending approximately from the microgram scale, 10^{-9} kg, to the mass of the Sun, $M_\odot \simeq 2 \times 10^{30}$ kg. This interval spans nearly forty orders of magnitude in mass. The lower scale is chosen conservatively so that the objects can be treated unambiguously as macroscopic classical bodies, without requiring a quantum description of their collective state. The upper scale remains safely within the weak-field domain for ordinary material densities, where the equivalent compact configuration remains far outside its Schwarzschild radius. This provides a broad classical domain in which the construction can be established directly from Newtonian gravity before considering its continuation into the relativistic regime.

Consider two bodies of masses m and M, radii r and R, and volumes:

$$v = \frac{4\pi r^3}{3} \qquad V = \frac{4\pi R^3}{3}$$

We define a compact reference configuration by conserving both total mass and total constituent volume:

$$M_t = m + M \qquad V_t = V + v = \frac{4\pi}{3}(R^3 + r^3)$$

The corresponding equivalent radius is:

$$R_t = (R^3 + r^3)^{1/3}$$

If the two bodies have the same volumetric density, the compact body has the same density:

$$\frac{m}{v} = \frac{M}{V} = \frac{M_t}{V_t}$$

If their densities differ, conservation of total mass and total volume uniquely determines the effective density of the equivalent compact sphere.

Within this Newtonian weak-field domain, the gravitational potential energy of a homogeneous solid sphere is given by:

$$E_p = -\frac{3GM^2}{5R} \tag{2}$$

The gravitational binding-energy scale can then be evaluated by comparing the compact and separated configurations, their energies are denoted directly by:

$$E_{\text{compact}} = -\frac{3GM_t^2}{5R_t} \tag{3}$$

$$E_{\text{separated}} = -\frac{3GM^2}{5R} - \frac{3Gm^2}{5r} - \frac{GMm}{d} \tag{4}$$

The corresponding energy difference is:

$$\Delta E_p = E_{\text{separated}} - E_{\text{compact}} \tag{5}$$

$$= \left(-\frac{3GM^2}{5R} - \frac{3Gm^2}{5r} - \frac{GMm}{d}\right) + \frac{3GM_t^2}{5R_t} \tag{6}$$

With this convention, ΔE_p is the energy required to transform the compact configuration into the separated configuration. Conversely, when the separated bodies fall toward one another under their mutual gravitational attraction and undergo a perfectly inelastic aggregation, the same positive quantity is released. During the infall, the decrease in gravitational potential energy is converted into kinetic energy. Because the constituent volumes and internal structures are conserved in the present construction, this energy cannot be retained through compression, deformation, or heating of the final configuration and must instead be carried away from the system as radiation, principally electromagnetic or gravitational radiation. The compact configuration therefore provides a direct physical interpretation of ΔE_p as the gravitational energy released by the hypothetical aggregation of the two bodies.

Mass and volume conservation are used here to define a unique compact reference configuration. They do not imply that all microscopic interactions within an actual material aggregate vanish. Rather, the construction isolates the gravitational contribution by comparing configurations with identical total mass and constituent volume while retaining only gravitational energy in the energy balance.

The derivation above establishes the functional form of the binding-energy expression over nearly forty orders of magnitude within a classical weak-field domain. At sufficiently large mass and compactness, the equivalent compact radius eventually approaches the Schwarzschild scale and its Newtonian derivation can no longer provide the appropriate physical justification. As shown later, however, this change of regime does not require a change in the resulting functional form. An independent relativistic treatment recovers the same expression in the regime where the compact reference configuration can no longer be interpreted purely within Newtonian gravity.

1.2 Mass-equivalent gravitational binding energy

The gravitational binding energy defined above is a physical energy difference between two configurations of the same system. In the aggregation process, this energy can be released from the system and therefore enters the energy balance in the same way as any other form of energy. Its gravitational origin does not prevent it from being expressed through the mass–energy equivalence relation $E = mc^2$.

In general relativity, the gravitational field produced by a system is determined by its total mass–energy content rather than by the sum of the rest masses of its constituents alone. Changes in the energy content of the system therefore change its gravitational field. If an amount of energy ΔE_p is released from or added to the system, the corresponding change in its gravitating mass is naturally expressed as:

$$M_{B_E} = \frac{\Delta E_p}{c^2} \tag{7}$$

This representation does not introduce an additional material component. It expresses the gravitational binding-energy contribution in units of mass. From the gravitational point of view, an increase or decrease in the total energy of an isolated system changes the mass parameter governing its external gravitational field by the corresponding amount E/c^2. The resulting contribution to spacetime curvature is therefore observationally equivalent, at the level of the gravitational mass being measured, to the curvature associated with the same amount of mass-energy.

Gravitational energy nevertheless has a particular status in general relativity. Unlike matter energy, it cannot in general be represented by a unique local energy density that is independent of coordinates and observers. Its contribution is instead encoded in the global or quasi-local mass-energy of the gravitating system. This is reflected in relativistic mass constructions such as the Hawking mass, the Misner–Sharp mass, and related quasi-local definitions [13, 15, 21].

A particularly relevant comparison is provided by the gravitational self-interaction approach developed by Deur [8, 9]. Starting from the nonlinear self-coupling of the gravitational field inherent to General Relativity, this approach finds that field self-interaction increases the gravitational binding of massive systems and can reproduce part of the gravitational response conventionally attributed to dark matter. The resulting excess gravitational effect can therefore be expressed as an effective dark mass without introducing an additional material component.

This raises the possibility that the self-interaction contribution calculated by Deur and the gravitational potential-energy contribution considered here represent two descriptions of the same underlying gravitational energy. Such an equivalence is physically plausible but has not, to our knowledge, been demonstrated explicitly. In particular, Deur's calculations determine the modification of the gravitational field and the resulting dynamics from gravitational self-interaction, whereas the present approach evaluates the corresponding energy through a binding-energy formulation.

An important distinction is that the self-interaction calculations do not directly provide a simple closed analytical expression for this energy contribution in terms of the masses and volumes of the constituents. The formulation developed here yields such an estimator directly through the gravitational binding-energy difference. Establishing whether the two formulations are quantitatively equivalent would therefore provide a direct connection between the approaches and clarify whether they describe the same underlying gravitational-energy contribution.

The quantity M_{B_E} therefore provides the natural mass representation of the gravitational binding energy defined in the preceding section. It allows this energy contribution to be compared directly with baryonic mass and with the additional gravitating mass inferred from galactic dynamics, without interpreting it as a new form of matter.

The physical existence of a potential-energy difference does not depend on whether the corresponding transformation occurs spontaneously. A stable system may remain indefinitely in its present configuration while still possessing a real energy difference relative to another physically accessible configuration. Nuclear fission provides a familiar example. Uranium nuclei contained in a stable mineral do not need to undergo spontaneous fission for the corresponding nuclear energy difference to be real. If fission is induced, measurable energy is released. The same principle applies to nuclear fusion and, at a more elementary scale, to an object resting on a table. Its stable position does not eliminate its gravitational potential energy, which becomes manifest if the object is allowed to fall.

The same reasoning applies to a stationary or collisionless gravitational system. The absence of an ongoing aggregation does not eliminate the energy difference between the distributed and compact configurations. If the bodies are allowed to fall toward one another and aggregate, this energy becomes physically manifest through the corresponding release of gravitational energy. The existence of the binding-energy difference therefore does not require the system to have previously undergone the transformation.

1.3 Newtonian examples of gravitational binding energy

To illustrate the magnitude of the gravitational binding energy defined above, we consider three familiar systems that are accurately described within Newtonian gravity: the Moon–Earth, Earth–Sun, and Jupiter–Sun systems. These examples compare the observed separated configuration with the corresponding hypothetical volume-conserving compact configuration and quantify the associated gravitational energy difference.

The smaller and larger bodies have masses m and M, radii r and R, and separation d. The compact configuration has total mass $M_t = m + M$ and radius $R_t = (R^3 + r^3)^{1/3}$, obtained by conserving the combined volume of the two bodies. Table 1 summarizes the physical parameters used in the calculation.

Table 1: Physical parameters used for the three Newtonian binding-energy examples. The compact reference radius R_t is obtained by conserving the combined volume of the two bodies.

System	m (kg)	M (kg)	r (m)	R (m)	d (m)	R_t (m)
Moon–Earth	$7.35 \cdot 10^{22}$	$5.97 \cdot 10^{24}$	$1.74 \cdot 10^{6}$	$6.38 \cdot 10^{6}$	$3.8 \cdot 10^{8}$	$6.42 \cdot 10^{6}$
Earth–Sun	$5.97 \cdot 10^{24}$	$1.99 \cdot 10^{30}$	$6.38 \cdot 10^{6}$	$6.96 \cdot 10^{8}$	$1.5 \cdot 10^{11}$	$6.96 \cdot 10^{8}$
Jupiter–Sun	$1.90 \cdot 10^{27}$	$1.99 \cdot 10^{30}$	$6.99 \cdot 10^{7}$	$6.96 \cdot 10^{8}$	$7.8 \cdot 10^{11}$	$6.97 \cdot 10^{8}$

For each system, the energy difference is $\Delta E_p = E_{\text{separated}} - E_{\text{compact}}$, and its mass equivalent is $M_{B_E} = \Delta E_p/c^2$. The resulting values are shown in Table 2. The final column gives the mass-equivalent binding energy relative to the mass m of the smaller body.

Table 2: Gravitational energy differences between the observed separated configurations and their hypothetical volume-conserving compact configurations. The mass-equivalent contribution is $M_{B_E} = \Delta E_p/c^2$, while M_{B_E}/m expresses this global gravitational energy scale relative to the smaller body.

System	E_{compact} (J)	$E_{\text{separated}}$ (J)	ΔE_p (J)	M_{B_E} (kg)	M_{B_E}/m
Moon–Earth	$-2.2795 \cdot 10^{32}$	$-2.2413 \cdot 10^{32}$	$3.8176 \cdot 10^{30}$	$4.2477 \cdot 10^{13}$	$5.8 \cdot 10^{-10}$
Earth–Sun	$-2.2751 \cdot 10^{41}$	$-2.2751 \cdot 10^{41}$	$1.3024 \cdot 10^{36}$	$1.4491 \cdot 10^{19}$	$2.4 \cdot 10^{-6}$
Jupiter–Sun	$-2.2787 \cdot 10^{41}$	$-2.2751 \cdot 10^{41}$	$3.5519 \cdot 10^{38}$	$3.9520 \cdot 10^{21}$	$2.1 \cdot 10^{-6}$

The magnitude of these energies is easier to appreciate on a familiar physical scale. The hypothetical aggregation of the Moon with the Earth corresponds to approximately $3.82 \cdot 10^{30}$ J. Using a large thermonuclear explosion as a reference, this is equivalent to roughly 40 trillion hydrogen bombs. Through mass–energy equivalence, the same gravitational energy corresponds to approximately $4.25 \cdot 10^{13}$ kg.

The Earth–Sun system reaches approximately $1.30 \cdot 10^{36}$ J, corresponding to a mass equivalent of $1.45 \cdot 10^{19}$ kg, while the Jupiter–Sun example reaches $3.55 \cdot 10^{38}$ J and $3.95 \cdot 10^{21}$ kg. These examples show that even familiar Newtonian gravitational systems involve extremely large absolute binding energies despite their small contribution relative to the total material mass.

The Earth–Sun value is particularly interesting because a mass-equivalent contribution of order 10^{19} kg is not intrinsically negligible on terrestrial gravitational scales. Depending on the spatial distribution of the gravitational binding-energy contribution within the Earth–Sun system, its gravitational effect could in principle be measurable in the terrestrial environment. The scalar energy value alone, however, does not determine the magnitude of such a local effect.

The gravitational binding energy belongs to the interacting system as a whole and cannot be uniquely partitioned between its two components. Nevertheless, expressing this energy relative to either mass provides a meaningful measure of the gravitational energy scale associated with that body. For the ordinary interaction term $U = -GmM/d$, normalization by the smaller body gives $|U|/m = GM/d$, whereas normalization by the larger body gives $|U|/M = Gm/d$. The ratio between these two specific energy scales is therefore M/m.

When $M \gg m$, the same gravitational interaction consequently represents a much larger energy scale relative to the smaller body's own mass. This does not imply that the interaction energy is localized within the smaller body. The energy remains a property of the complete interacting configuration, while the normalization reflects that the smaller body is embedded in a gravitational environment dominated by the larger mass.

The ratio M_{B_E}/m in Table 2 has the same interpretation. It measures the mass-equivalent gravitational binding energy of the complete system relative to the mass scale of the smaller body, rather than assigning that energy specifically to the smaller body.

1.4 Quasi-localization of gravitational binding energy

An important question concerns where the gravitational binding energy of a system should be associated. For a system of n bodies, the binding energy results from interactions between bodies belonging to the same bounded system. It is therefore natural to associate this energy with a closed surface enclosing these bodies, rather than with any individual body.

General relativity gives a precise meaning to this idea through quasi-local energy. Gravitational energy does not possess a unique covariant pointwise density, but several relativistic constructions associate the total mass–energy of a bounded region with its enclosing two-surface [14, 25]. In spherical symmetry this statement becomes particularly clear. The Misner–Sharp energy measures the energy enclosed by a spherical surface and remains constant through a surrounding Schwarzschild vacuum region. This is consistent with Birkhoff's theorem, according to which the exterior geometry of a spherically symmetric isolated system is determined by the mass enclosed within it.

The spherical construction used below should not be interpreted as an assumption that a galaxy itself is spherical. In a disk galaxy, matter outside a given cylindrical radius can contribute to the radial gravitational field. The relevant quantity can nevertheless be expressed through the spherically equivalent mass associated with the circular velocity:

$$M_{\text{eq}}(R) = \frac{RV^2(R)}{G} \tag{8}$$

This quantity is the spherical mass that would generate the same radial acceleration at R. The baryonic rotation velocity already contains the effect of the actual baryonic distribution, so that:

$$M_{\text{bar,eq}}(R) = \frac{RV_{\text{bar}}^2(R)}{G} \tag{9}$$

provides an equivalent radial representation without requiring spherical baryonic geometry.

The same representation can be applied to the effective mass associated with gravitational binding energy. At each radius, the radial dynamics can therefore be described by the equivalent baryonic source and by the effective mass associated with the binding energy attributed to that quasi-local scale. Binding energy associated with a larger configuration belongs to the corresponding larger quasi-local region and is not assigned retrospectively to smaller radii.

2 Newtonian gravitational binding energy

The first observation is that the interaction term $-GmM/d$ in ΔE_p becomes negligible compared with the internal self-energy terms in gravitational systems characterized by large scale separation. Relative to the dominant term GM^2/R, its magnitude is $(GMm/d)/(GM^2/R) = (m/M)(R/d)$. For elementary astrophysical bodies such as planets and stars, both $m/M \ll 1$ and $R/d \ll 1$, so this contribution is generally very small.

The same scale separation persists when the construction is extended hierarchically. Bound objects occupy only a small fraction of the volume associated with their mutual separation. If the constituent volumes are combined under volume conservation, the corresponding effective radius scales as $N^{1/3}$. The characteristic separation scale grows approximately in the same way, so their ratio remains small across successive aggregation levels. For a Milky Way–type galaxy, combining the stellar volumes gives an effective occupied radius much smaller than characteristic interstellar distances, with $R/d \sim 10^{-4}$.

At galactic masses, the resulting volume-conserving compact configuration can lie beyond the regime in which it may be interpreted physically within Newtonian gravity. This does not affect the preceding scale-separation argument, since the effective radius is used here only as a geometrical measure of the conserved constituent volume. No Newtonian binding energy is inferred from the hypothetical compact galactic configuration at this stage.

The effective binding-energy contribution considered here is therefore not obtained by assigning a positive mass to the conventional pairwise term $-GmM/d$. In the hierarchical regime, this term becomes subdominant and the dominant contribution arises from the compact-reference self-energy terms proportional to M^2/R. To leading order, the two-body energy difference becomes:

$$\Delta E_p = \frac{3G}{5}\left(\frac{M_t^2}{R_t} - \alpha_M\frac{M^2}{R} - \alpha_m\frac{m^2}{r}\right) \tag{10}$$

where α_M and α_m describe the internal mass distributions of the two bodies. For homogeneous spheres $\alpha = 1$, while more generally $\alpha \sim \mathcal{O}(1)$ depends on the density profile.

Consider now a system of n bodies with masses m_i, radii r_i, and internal coefficients α_i, successively aggregated under volume conservation. After the ith aggregation, the cumulative mass is $M_i = \sum_{j \le i} m_j$ and the effective radius satisfies $R_i^3 = R_{i-1}^3 + r_i^3$. The corresponding energy difference is:

$$\Delta E_i = \frac{3G}{5}\left(\frac{M_i^2}{R_i} - \frac{M_{i-1}^2}{R_{i-1}} - \alpha_i \frac{m_i^2}{r_i}\right), \qquad \Delta E_p = \sum_{i=1}^{n} \Delta E_i \tag{11}$$

The sum is telescopic, so all intermediate compact-state terms cancel and only the final collective contribution and the initial internal contributions remain:

$$\Delta E_p = \frac{3G}{5}\left[\frac{M_n^2}{R_n} - \sum_{i=1}^{n} \alpha_i \frac{m_i^2}{r_i}\right] \tag{12}$$

with $M_n = \sum_i m_i$ and $R_n = (\sum_i r_i^3)^{1/3}$. The first term therefore depends only on the total mass and total conserved volume of the system, while the second retains the internal binding contributions of the individual bodies. As shown below, these individual contributions become asymptotically subdominant for large systems and cancel exactly when the intrinsic binding energies of the constituents are restored.

The compact volume-conserving configuration represents the maximally aggregated state considered in this construction while preserving the internal volumes and structures of the constituents. It may be viewed as a configuration in which the bodies are placed side by side without compression. Volume conservation is essential because further contraction would introduce additional non-gravitational forces, such as degeneracy pressure, radiation pressure, or material stresses, into the energy balance. By excluding such compression, the construction isolates the gravitational contribution to the energy difference between the separated and aggregated configurations.

2.1 Proof of permutation invariance

The final result must also be independent of the order in which the bodies are aggregated. Let σ be any permutation of $\{1, \ldots, n\}$. Applying Equation (12) to this ordering gives:

$$\Delta E_p(\sigma) = \frac{3G}{5}\left[\frac{\left(\sum_{i=1}^{n} m_{\sigma(i)}\right)^2}{\left(\sum_{i=1}^{n} r_{\sigma(i)}^3\right)^{1/3}} - \sum_{i=1}^{n} \alpha_{\sigma(i)} \frac{m_{\sigma(i)}^2}{r_{\sigma(i)}}\right] \tag{13}$$

Each sum is invariant under permutation, so $\Delta E_p(\sigma) = \Delta E_p$. The binding-energy difference is therefore independent of the aggregation order. ■

2.2 Simplified calculation with identical bodies

Consider n identical bodies of mass m, radius r, and internal structure characterized by a coefficient α. After the ith aggregation, the cumulative mass is $M_i = im$. Since volume is conserved and all bodies have the same density, the corresponding effective radius is $R_i = i^{1/3} r$.

The energy released at each aggregation step is:

$$\Delta E_i = \frac{3G}{5}\left(\frac{M_i^2}{R_i} - \frac{M_{i-1}^2}{R_{i-1}} - \alpha\frac{m^2}{r}\right), \qquad \Delta E_p = \sum_{i=1}^{n} \Delta E_i \tag{14}$$

The intermediate compact-state terms cancel telescopically, leaving:

$$\Delta E_p = \frac{3G}{5}\left(\frac{M_n^2}{R_n} - \alpha n\frac{m^2}{r}\right) = \frac{3G}{5}\left(n^{5/3} - \alpha n\right)\frac{m^2}{r} \tag{15}$$

where $M_n = nm$ and $R_n = n^{1/3} r$. The collective contribution therefore scales as $n^{5/3}$, whereas the term associated with the internal binding energies of the individual bodies scales only as n. Their relative magnitude is $\alpha n^{-2/3}$ and consequently vanishes for $n \gg 1$.

The internal-structure contribution is therefore asymptotically negligible in the assembly energy. The dominant term is the collective contribution M_n^2/R_n, showing that at large n the gravitational binding energy is governed primarily by the total mass and effective radius rather than by the internal structure of the individual constituents.

There is, however, a second and stronger cancellation. The quantity ΔE_p represents the energy released by assembling the n bodies, but each body already possesses its own intrinsic gravitational binding energy. The total intrinsic contribution of the initial bodies is $(3G/5)\alpha n m^2/r$. Restoring this energy in the total balance gives:

$$E_{\text{tot}} = \Delta E_p + \frac{3G}{5}\alpha n\frac{m^2}{r} = \frac{3G}{5}\frac{M_n^2}{R_n} \tag{16}$$

Thus, the contribution associated with the internal structures of the elementary bodies disappears in two complementary ways. First, it is asymptotically suppressed relative to the collective contribution as $n^{-2/3}$. Second, when the intrinsic binding energies of the initial bodies are included in the complete energy balance, the same term cancels exactly.

The final result is therefore independent of α and identical to the gravitational binding energy of a homogeneous self-gravitating sphere with total mass M_n and volume-conserving radius R_n. The result does not depend on the detailed internal structure of the identical constituents, but only on the global mass and volume of the aggregated system.

2.3 Generalization to arbitrary distributions

The previous result does not require identical bodies. Consider n constituents with masses m_i, radii r_i, and internal-structure coefficients α_i. Under volume conservation, the cumulative quantities are $M_i = \sum_{j=1}^{i} m_j$ and $R_i = (\sum_{j=1}^{i} r_j^3)^{1/3}$. The telescoping sum derived above therefore gives:

$$\Delta E_p = \frac{3G}{5}\left[\frac{\left(\sum_{i=1}^{n} m_i\right)^2}{\left(\sum_{i=1}^{n} r_i^3\right)^{1/3}} - \sum_{i=1}^{n} \alpha_i \frac{m_i^2}{r_i}\right] \tag{17}$$

This expression is deterministic and does not assume any particular distribution of masses, radii, or internal structures. The constituents may therefore follow normal, log-normal, truncated, empirical, stellar-mass-function, or other distributions for which the relevant moments exist. No independence between mass and radius is required for Equation (17).

If the constituents are regarded as random variables drawn from a statistically homogeneous population, the large-n behavior follows from $\sum_i m_i \simeq n\langle m\rangle$ and $\sum_i r_i^3 \simeq n\langle r^3\rangle$. The collective term then scales as $n^{5/3}\langle m\rangle^2/\langle r^3\rangle^{1/3}$, whereas the internal contribution scales as $n\langle \alpha m^2/r\rangle$. Hence:

$$\mathbb{E}[\Delta E_p] \simeq \frac{3G}{5}\left[n^{5/3}\frac{\langle m\rangle^2}{\langle r^3\rangle^{1/3}} - n\left\langle \alpha\frac{m^2}{r}\right\rangle\right] \tag{18}$$

The ratio of the internal contribution to the collective contribution is therefore proportional to $n^{-2/3}$, with coefficient $\langle \alpha m^2/r\rangle\langle r^3\rangle^{1/3}/\langle m\rangle^2$. For finite moments and $\alpha \sim \mathcal{O}(1)$, this ratio vanishes as $n \to \infty$. The asymptotic suppression obtained for identical bodies therefore persists for arbitrary component distributions.

For multimodal distributions, the same deterministic expression remains valid. The different modes may be interpreted as distinct subpopulations and treated either through their mixture distribution or by summing their contributions explicitly.

The second protection also remains exact. Restoring the intrinsic binding energies of all initial constituents gives:

$$E_{\text{tot}} = \Delta E_p + \frac{3G}{5}\sum_{i=1}^{n}\alpha_i\frac{m_i^2}{r_i} = \frac{3G}{5}\frac{\left(\sum_{i=1}^{n} m_i\right)^2}{\left(\sum_{i=1}^{n} r_i^3\right)^{1/3}} \tag{19}$$

Thus, the same double protection found for identical bodies applies to arbitrary distributions. The internal-structure contribution is asymptotically suppressed as $n^{-2/3}$ in the assembly energy and cancels exactly in the total binding energy. The final result therefore depends only on the total mass and volume-conserving effective radius of the aggregated system, rather than on the detailed internal structure of its individual constituents.

2.4 Derivation of the full binding-energy formula

The previous results can now be applied hierarchically to the stellar populations of a galaxy. For each stellar class i, let M_i, V_i, and R_i denote its total mass, total constituent volume, and corresponding effective radius. If v_{ik} is the volume of the kth star in the class, then $V_i = \sum_{k=1}^{N_i} v_{ik} \simeq N_i \langle v \rangle_i$. Defining the effective class density as $\rho_i = M_i/V_i \simeq \langle m \rangle_i / \langle v \rangle_i$ gives:

$$R_i = \left(\frac{3M_i}{4\pi \rho_i} \right)^{1/3} \tag{20}$$

Equation (19) then gives the binding energy associated with each homogeneous stellar class. Summing over all classes gives the class-level contribution:

$$E_{\text{sum}} = \frac{3G}{5} \sum_{i=1}^{n} \frac{M_i^2}{R_i} \tag{21}$$

These class-level energies are already part of the hierarchical system and remain present when the classes are subsequently aggregated. The next level therefore adds the gravitational binding energy associated with combining these class-level subsystems rather than replacing their existing binding energies.

In principle, this additional contribution could be evaluated from all $(n^2 - n)/2$ gravitational relations between the class-level subsystems. When a large number of such subsystems is distributed without a preferred ordering, the continuum limit gives the same functional dependence as a compact homogeneous configuration with total mass $M = \sum_i M_i$ and volume-conserving radius $R = (\sum_i R_i^3)^{1/3}$. The corresponding global aggregation contribution is therefore $(3G/5)M^2/R$.

The complete Newtonian hierarchical binding energy is consequently:

$$E_p = \frac{3G}{5} \left[\sum_{i=1}^{n} \frac{M_i^2}{R_i} + \frac{M^2}{R} \right] \tag{22}$$

The first term is the binding energy already contained in the homogeneous class-level subsystems, while the second is the additional energy associated with their global aggregation. The two terms therefore correspond to two successive levels of the same hierarchical construction.

Each class-level aggregation formally also contains the intrinsic stellar terms proportional to $\sum_j m_{ij}^2 / r_{ij}$. As shown in Sections 2.2 and 2.3, these contributions are asymptotically suppressed as $N^{-2/3}$ and cancel exactly when the intrinsic binding energies of the constituent stars are restored. They therefore do not appear as independent terms in Equation (22).

The global contribution does not depend on the number of stellar classes used to represent the galaxy. The classes provide a finite parametrization of the stellar population, whereas the term M^2/R represents the continuum-limit aggregation of the underlying gravitational subsystems.

2.5 Relativistic limit of the Newtonian construction

The hierarchical expression derived above has a recursive interpretation. If a system S is assembled from already bound subsystems S_i, the binding energies of these subsystems remain part of the final energy balance, while the next hierarchical level adds the binding energy associated with their collective aggregation. Repeating the construction therefore preserves the contributions acquired at each preceding level rather than replacing them.

This Newtonian construction nevertheless has a definite limit of applicability. For a compact configuration of mass M and radius R, the binding-energy scale $B_E = (3G/5)M^2/R$ corresponds through mass–energy equivalence to $M_{B_E} = B_E/c^2$. Introducing the Schwarzschild radius $R_s = 2GM/c^2$ gives:

$$\frac{M_{B_E}}{M} = \frac{3}{10}\frac{R_s}{R} \tag{23}$$

As R approaches R_s, gravitational self-energy is no longer a small contribution to the total mass–energy budget and the weak-field Newtonian description cannot be extrapolated further. For a static, spherically symmetric and isotropic fluid configuration, the Buchdahl bound $R > 9R_s/8$ gives the stronger consistency condition:

$$\frac{M_{B_E}}{M} < \frac{4}{15} \tag{24}$$

The compact volume-conserving configuration must therefore cease to be interpreted as a Newtonian material state before arbitrarily large binding energies are reached.

The recursive construction also admits a useful limiting interpretation through successive black-hole absorption. Before crossing the horizon, each bound subsystem carries its own mass–energy contribution. After absorption, its internal structure and assembly history are no longer independently observable, as expressed by the no-hair property, but energy conservation requires its contribution to remain part of the total mass–energy of the final object. The disappearance of observable substructure therefore provides no reason to erase contributions acquired at earlier hierarchical levels.

This suggests that the recursive structure obtained in the Newtonian regime should remain unchanged as successive aggregation enters the relativistic regime. The following derivation uses a density-equivalent gravitational length scale associated with each stellar class to evaluate the energy carried through successive absorption. This scale is defined from the equality of mean densities and does not require the existence of a material boundary or a physical tidal-disruption surface at the corresponding radius. The derivation does not constitute a treatment formulated entirely within General Relativity, but, as shown below, it independently recovers the same functional form obtained from the purely Newtonian construction.

3 Binding-energy derivation in the relativistic regime

Consider the sequential absorption by a black hole of stars belonging to a stellar population class i with common intrinsic mean density ρ_i. At a given stage of the process, let $\mathcal{M}$ denote the mass already incorporated into the absorbing black hole, and consider an additional star of mass $m_\star$ and radius $r_\star$, with $\rho_i = 3m_\star/(4\pi r_\star^3)$.

For each incoming star, we define a density-equivalent tidal scale $r_{t,i}$ by equating the mean density associated with the accumulated black-hole mass $\mathcal{M}$ inside this scale to the intrinsic mean density of the stellar class:

$$\frac{\mathcal{M}}{r_{t,i}^3} = \frac{m_\star}{r_\star^3}$$

Using $\rho_i = 3m_\star/(4\pi r_\star^3)$ gives:

$$r_{t,i}(\mathcal{M}) = \left(\frac{3\mathcal{M}}{4\pi\rho_i}\right)^{1/3}$$

The density-equivalent tidal scale therefore depends on the accumulated black-hole mass and on the intrinsic density of the stellar class, but not on the individual stellar mass. It is an equivalent gravitational length scale defined by the density relation above and need not correspond to a physical tidal-disruption surface or to a material boundary of the absorbing system.

Using this density-equivalent scale, the corresponding gravitational-energy increment is:

$$dE_{p,i} = \frac{G\mathcal{M}}{r_{t,i}(\mathcal{M})}\, d\mathcal{M} = G\left(\frac{4\pi\rho_i}{3}\right)^{1/3} \mathcal{M}^{2/3} d\mathcal{M} \tag{25}$$

For a stellar class containing a sufficiently large number of constituents, the sequential absorption can be represented in the continuum limit. Integrating from zero accumulated mass to the total class mass M_i, and defining the intrinsic volume-equivalent radius $R_i = (3M_i/4\pi\rho_i)^{1/3}$, gives:

$$\begin{aligned} E_{p,i} &= G\left(\frac{4\pi\rho_i}{3}\right)^{1/3} \int_0^{M_i} \mathcal{M}^{2/3} d\mathcal{M} \\ &= \frac{3G}{5}\frac{M_i^2}{R_i} \end{aligned} \tag{26}$$

The M_i^2/R_i dependence is therefore recovered without requiring the stellar population to form a compact material sphere. The factor 3/5 follows from the accumulation of gravitational energy evaluated through the density-equivalent scale defined above. The construction depends only on the relation between the accumulated mass and the intrinsic density of the stellar class; it does not require $r_{t,i}$ to represent a physical disruption surface.

If the density-equivalent scale is related to a more detailed physical tidal-disruption prescription, stellar structure, orbital properties, and the precise disruption criterion may introduce an order-unity factor ξ_i, such that:

$$r_{t,i} = \xi_i \left(\frac{3\mathcal{M}}{4\pi\rho_i}\right)^{1/3}$$

The same calculation then gives:

$$E_{p,i} = \xi_i^{-1} \frac{3G}{5} \frac{M_i^2}{R_i}$$

The density-equivalence definition $\mathcal{M}/r_{t,i}^3 = m_\star/r_\star^3$ corresponds exactly to $\xi_i = 1$, rather than to an independently fitted normalization. The functional dependence $E_{p,i} \propto M_i^{5/3}\rho_i^{1/3} = M_i^2/R_i$ is therefore unchanged by such order-unity modifications of the equivalent scale.

The result is independent of the absorption order. For a finite sequence, the contribution associated with the ath absorbed constituent is proportional to $\mathcal{M}_a^{5/3} - \mathcal{M}_{a-1}^{5/3}$, where $\mathcal{M}_a$ is the accumulated mass after that absorption. The complete sum therefore telescopes and depends only on the final class mass M_i. The continuum integral represents the same order-independent accumulation.

Summing over the stellar population classes gives:

$$E_{p,\text{class}} = \frac{3G}{5} \sum_{i=1}^{n} \frac{M_i^2}{R_i} \tag{27}$$

3.1 Collective derivation of the global binding term

The class-level derivation applies independently to populations of common intrinsic density. The next hierarchical level combines classes with different intrinsic densities and therefore cannot be represented by a single class density-equivalent scale. Define the total mass as $M = \sum_i M_i$ and the intrinsic volume-equivalent radius by $R^3 = \sum_i R_i^3$. This radius is not the physical radius of the galaxy or a disk scale length; it is defined exclusively by the conserved intrinsic volumes of its stellar constituents.

Because the global binding contribution is a state function, it may be evaluated along a convenient self-similar assembly path. Let $M_i(\lambda) = \lambda M_i$ with $0 \le \lambda \le 1$ while the intrinsic densities remain fixed. It follows directly that $M(\lambda) = \lambda M$ and $R(\lambda) = \lambda^{1/3} R$. The collective gravitational work is then:

$$E_{p,\text{global}} = \int_0^1 \frac{GM(\lambda)}{R(\lambda)}\, dM(\lambda) = \frac{GM^2}{R} \int_0^1 \lambda^{2/3} d\lambda = \frac{3G}{5}\frac{M^2}{R} \tag{28}$$

The factor 3/5 therefore follows from the same mass–volume scaling as in the class-level calculation. It does not require the galaxy itself to occupy a homogeneous spherical configuration; the radius R represents only the intrinsic volume scale entering the collective hierarchical degree of freedom.

Combining the independently derived class-level and global contributions gives:

$$E_p = \frac{3G}{5}\left[\sum_{i=1}^{n}\frac{M_i^2}{R_i} + \frac{M^2}{R}\right] \tag{29}$$

This construction can remain applicable when the final absorbing system lies in the relativistic regime because no Newtonian material configuration with an effective radius below its own Schwarzschild radius is required. The density-equivalent scale used in the class-level derivation is a gravitational reference scale defined from the intrinsic stellar density and the accumulated mass; it is not required to correspond to a physical material surface or to an externally accessible tidal-disruption radius. The actual absorption process belongs to the relativistic regime, while the density-equivalent construction determines the gravitational-energy scaling carried into that process. The resulting functional form is therefore identical to that obtained independently from the purely Newtonian hierarchical derivation.

4 Mass-fraction form of the binding-energy equation

The binding-energy expression derived above contains two distinct contributions, the class-level term and the global aggregation term. To keep these contributions explicit in the following analytical developments, we write:

$$E_p = \frac{3G}{5}\left[\alpha\sum_{i=1}^{n}\frac{M_i^2}{R_i} + \beta\frac{M^2}{R}\right] \tag{30}$$

where α and β identify the class-level and global contributions, respectively. The physical derivation obtained above corresponds to $\alpha = \beta = 1$.

Let the mass fraction of stellar class i be $\phi_i = M_i/M$, so that $M_i = \phi_i M$ and $\sum_i \phi_i = 1$. Since $R_i = (3M_i/4\pi\rho_i)^{1/3}$, the class-level contribution becomes:

$$\sum_{i=1}^{n}\frac{M_i^2}{R_i} = \left(\frac{4\pi}{3}\right)^{1/3} M^{5/3}\sum_{i=1}^{n}\rho_i^{1/3}\phi_i^{5/3} \tag{31}$$

For the global contribution, volume conservation gives $R^3 = \sum_i R_i^3$. Using $R_i^3 = 3M_i/(4\pi\rho_i)$ and $M_i = \phi_i M$ gives $R^3 = (3M/4\pi)\sum_i \phi_i/\rho_i$, and consequently:

$$\frac{M^2}{R} = \left(\frac{4\pi}{3}\right)^{1/3} M^{5/3}\left(\sum_{i=1}^{n}\frac{\phi_i}{\rho_i}\right)^{-1/3} \tag{32}$$

Substituting both contributions into Equation (30) gives:

$$E_p(M, \boldsymbol{\phi}; \alpha, \beta) = \frac{3G}{5}\left(\frac{4\pi}{3}\right)^{1/3} M^{5/3}\left[\alpha \sum_{i=1}^{n} \rho_i^{1/3}\phi_i^{5/3} + \beta\left(\sum_{i=1}^{n}\frac{\phi_i}{\rho_i}\right)^{-1/3}\right] \tag{33}$$

For arbitrary constant coefficients α and β, the dependence on the total mass remains completely factorized as $M^{5/3}$. A remarkable consequence is that dividing the binding energy by this mass scale removes the dependence on the total baryonic mass:

$$\frac{E_p}{M^{5/3}} = \frac{3G}{5}\left(\frac{4\pi}{3}\right)^{1/3}\left[\alpha \sum_{i=1}^{n} \rho_i^{1/3}\phi_i^{5/3} + \beta\left(\sum_{i=1}^{n}\frac{\phi_i}{\rho_i}\right)^{-1/3}\right] \tag{34}$$

The normalized binding energy is therefore entirely determined by the stellar-population composition through the fractions ϕ_i and intrinsic densities ρ_i. The total baryonic mass controls only the overall $M^{5/3}$ amplitude. Equivalently, if the mass-equivalent contribution is written as $M_{B_E} = E_p/c^2$, then $M_{B_E}/M^{5/3}$ is also determined solely by the stellar population. Galaxies with the same stellar-population composition therefore have the same normalized binding-energy contribution independently of their total mass.

4.1 Loose analytical bounds

The mass-fraction form also provides population-independent bounds. Let $\rho_{\min} = \min_i \rho_i$ and $\rho_{\max} = \max_i \rho_i$, with $\phi_i \geq 0$ and $\sum_i \phi_i = 1$. For $\alpha \geq 0$ and $\beta \geq 0$, the two population-dependent terms satisfy $\sum_i \phi_i^{5/3} \in [n^{-2/3}, 1]$ and $\sum_i \phi_i/\rho_i \in [1/\rho_{\max}, 1/\rho_{\min}]$. Consequently:

$$\rho_{\min}^{1/3} n^{-2/3} \leq \sum_{i=1}^{n} \rho_i^{1/3}\phi_i^{5/3} \leq \rho_{\max}^{1/3} \tag{35}$$

and:

$$\rho_{\min}^{1/3} \leq \left(\sum_{i=1}^{n}\frac{\phi_i}{\rho_i}\right)^{-1/3} \leq \rho_{\max}^{1/3} \tag{36}$$

Using Equation (33), the binding energy is therefore bounded by:

$$\frac{3G}{5}\left(\frac{4\pi}{3}\right)^{1/3} M^{5/3}\rho_{\min}^{1/3}\left(\beta + \alpha n^{-2/3}\right) \leq E_p \leq \frac{3G}{5}\left(\frac{4\pi}{3}\right)^{1/3} M^{5/3}\rho_{\max}^{1/3}(\alpha + \beta) \tag{37}$$

These bounds require no knowledge of the stellar fractions themselves. They depend only on the total mass, the number of stellar classes, and the extreme intrinsic densities. The upper bound is attainable when all the mass belongs to the densest class, whereas the lower bound is generally conservative because the two contributions need not reach their minima for the same population mixture.

4.2 Tight bounds from convex optimization

Tighter bounds follow by optimizing the population-dependent part of Equation (33) directly over the stellar-population simplex. Defining:

$$K = \frac{3G}{5}\left(\frac{4\pi}{3}\right)^{1/3} \tag{38}$$

the binding energy can be written as:

$$E_p = M^{5/3}K\left[\alpha\sum_{i=1}^{n}\rho_i^{1/3}\phi_i^{5/3} + \beta\left(\sum_{i=1}^{n}\frac{\phi_i}{\rho_i}\right)^{-1/3}\right] \tag{39}$$

with $\phi_i \geq 0$ and $\sum_i \phi_i = 1$. For $\alpha, \beta \geq 0$, the population-dependent function is convex on the simplex: the first term is a non-negative weighted sum of the convex functions $\phi_i^{5/3}$, while the second is the convex function $x^{-1/3}$ applied to a positive affine function of $\boldsymbol{\phi}$.

The exact upper bound therefore occurs at a vertex of the simplex. If all the mass is placed in class j, the binding energy becomes $E_p = M^{5/3}K(\alpha+\beta)\rho_j^{1/3}$, giving:

$$E_{\max} = M^{5/3}K(\alpha+\beta)\rho_{\max}^{1/3} \tag{40}$$

which is identical to the analytical upper bound above.

The exact lower bound is the convex optimization problem:

$$E_{\min} = M^{5/3}K \min_{\phi_i\geq 0,\ \sum_i \phi_i = 1}\left[\alpha\sum_{i=1}^{n}\rho_i^{1/3}\phi_i^{5/3} + \beta\left(\sum_{i=1}^{n}\frac{\phi_i}{\rho_i}\right)^{-1/3}\right] \tag{41}$$

Because the objective is convex and the admissible population space is the unit simplex, any solution satisfying the Karush–Kuhn–Tucker conditions is a global minimum. The lower bound can therefore be obtained numerically without ambiguity from local minima.

Two limiting cases are analytical. For $\beta = 0$, minimization gives $\phi_i^* = \rho_i^{-1/2}/\sum_j \rho_j^{-1/2}$ and:

$$E_{\min} = M^{5/3}K\alpha\left(\sum_{i=1}^{n}\rho_i^{-1/2}\right)^{-2/3} \tag{42}$$

For $\alpha = 0$, the minimum is obtained by placing all the mass in the least dense class:

$$E_{\min} = M^{5/3} K \beta \rho_{\min}^{1/3} \tag{43}$$

For $\alpha, \beta > 0$, only the lower bound generally requires numerical minimization. Convexity guarantees that this minimum is globally tight within the adopted stellar-population simplex, while the upper bound remains analytical and exact.

5 Realistic bounds from stellar-population constraints

The loose and tight bounds derived above explore the stellar-population space without using prior information about the expected mass fractions. More realistic bounds can be obtained by restricting this space around representative stellar populations and their adopted uncertainties.

For each reference population, let f_i denote the central mass fraction of stellar class i and s_i its adopted 1σ uncertainty. The six populations considered here are Generic, Kroupa, Early, Intermediate, Late, and Irregular. Their adopted fractions and uncertainties are summarized in Table 3.

The reference populations used here are synthetic representative mixtures rather than direct measurements of individual galaxies. They were constructed from the broad stellar-population trends expected from the stellar initial mass function, stellar evolution and population synthesis, together with the observed evolution of stellar content and star formation along the galaxy morphological sequence [3, 5, 12, 16, 17]. The adopted fractions are therefore intended to define physically plausible reference populations and associated uncertainty domains, rather than unique population decompositions.

The adopted class densities are representative mean densities rather than universal values for each stellar type. They are based on characteristic stellar masses and radii and are intended to provide a common density scale for the population reconstruction. Main-sequence and evolved-star values are guided by empirical mass–radius determinations, while the compact-remnant values follow the characteristic mass–radius domains of white dwarfs and neutron stars [10, 11, 18, 27].

The intrinsic mean densities adopted for the stellar classes are listed in Table 4. These densities are fixed across all reference populations, while only the corresponding mass fractions and uncertainties vary. Black holes are excluded from the density-dependent calculation because they do not possess an intrinsic material density or stellar radius entering the tidal-work construction. In the present energy accounting, black-hole mergers do not introduce an additional potential-energy contribution. The energy emitted during the merger is accounted for by the difference between the initial and final mass-energy of the black-hole system. Black holes are therefore taken to contribute no additional gravitational potential energy to the global term considered here.

Table 3: Reference stellar-population mass fractions and adopted 1σ uncertainties. Values are expressed as percentages of the total population mass.

Class	Generic	Kroupa	Early	Intermediate	Late	Irregular
BH	1.00 ± 0.50	10.0 ± 3.0	1.20 ± 0.45	1.00 ± 0.30	0.70 ± 0.20	0.50 ± 0.20
NS	0.30 ± 0.10	5.00 ± 1.50	0.45 ± 0.20	0.30 ± 0.10	0.20 ± 0.08	0.20 ± 0.08
WD	2.20 ± 0.70	20.0 ± 4.0	5.00 ± 1.30	2.50 ± 0.60	1.50 ± 0.50	1.00 ± 0.40
RG	0.20 ± 0.10	1.00 ± 0.50	1.70 ± 0.575	0.30 ± 0.10	0.20 ± 0.08	0.10 ± 0.05
M	55.0 ± 10.0	38.0 ± 6.0	53.0 ± 5.5	55.0 ± 6.0	55.5 ± 6.0	56.0 ± 7.0
K	16.0 ± 6.0	16.0 ± 3.0	18.5 ± 3.5	17.0 ± 4.0	15.5 ± 4.0	14.0 ± 4.5
G	10.5 ± 5.0	5.00 ± 1.50	10.75 ± 2.50	10.5 ± 3.0	10.0 ± 3.0	9.00 ± 3.00
F	5.50 ± 3.00	2.50 ± 0.80	4.75 ± 1.80	5.50 ± 2.00	6.00 ± 2.20	6.00 ± 2.50
A	5.00 ± 2.00	1.00 ± 0.40	2.50 ± 1.10	4.00 ± 1.20	5.00 ± 1.50	5.50 ± 1.80
B	3.00 ± 1.00	1.00 ± 0.40	1.40 ± 0.70	2.50 ± 0.70	3.00 ± 1.00	4.00 ± 1.20
O	1.30 ± 0.50	0.50 ± 0.30	0.75 ± 0.40	1.40 ± 0.40	2.40 ± 0.60	3.70 ± 0.80

Table 4: Intrinsic mean densities adopted for the stellar population classes.

Class	BH	NS	WD	RG	M	K
ρ_i ($\mathrm{kg\,m^{-3}}$)	–	4.0×10^{17}	1.0×10^{9}	5.0×10^{-4}	9.0×10^{3}	2.4×10^{3}
Class	G	F	A	B	O	
ρ_i ($\mathrm{kg\,m^{-3}}$)	1.41×10^{3}	1.06×10^{3}	2.9×10^{2}	6.3×10^{1}	5.2×10^{1}	

Let I denote the remaining classes with $\rho_i > 0$ and let $S = \sum_{i \in I} f_i$. The fractions and uncertainties used in the binding-energy calculation are therefore normalized over these classes as $\bar{\phi}_i = f_i/S$ and $\sigma_i = s_i/S$.

For a chosen uncertainty width $k \geq 0$, each stellar fraction is restricted to:

$$\phi_i^- = \max\left(0, \bar{\phi}_i - k\sigma_i\right), \qquad \phi_i^+ = \min\left(1, \bar{\phi}_i + k\sigma_i\right) \tag{44}$$

while conservation of the total stellar mass requires $\sum_{i \in I} \phi_i = 1$. The admissible population domain is therefore:

$$\mathcal{P}_k = \left\{ \boldsymbol{\phi} \;:\; \phi_i^- \leq \phi_i \leq \phi_i^+, \quad \sum_{i \in I} \phi_i = 1 \right\} \tag{45}$$

which is non-empty only when $\sum_i \phi_i^- \leq 1 \leq \sum_i \phi_i^+$.

As in the preceding bounds, the dependence on total mass can be separated completely from the population-dependent factor. Using the constant K defined in Equation (38), the binding energy can be written as:

$$E_p = M^{5/3} K \left[\alpha \sum_{i \in I} \rho_i^{1/3} \phi_i^{5/3} + \beta \left(\sum_{i \in I} \frac{\phi_i}{\rho_i} \right)^{-1/3} \right] \tag{46}$$

The quantity bounded by the stellar population is independent of the total mass. We therefore define $P(\boldsymbol{\phi};\alpha,\beta)=E_p/M^{5/3}$. The realistic population bounds are then obtained by minimizing and maximizing P over the admissible domain $\mathcal{P}_k$:

$$P_{\min}^{(k)}=\min_{\boldsymbol{\phi}\in\mathcal{P}_k} P(\boldsymbol{\phi};\alpha,\beta), \qquad P_{\max}^{(k)}=\max_{\boldsymbol{\phi}\in\mathcal{P}_k} P(\boldsymbol{\phi};\alpha,\beta) \tag{47}$$

and the corresponding binding-energy interval for a system of mass M is simply $M^{5/3}P_{\min}^{(k)}\leq E_p\leq M^{5/3}P_{\max}^{(k)}$.

For $\alpha,\beta\geq 0$, the population function remains convex over the restricted domain $\mathcal{P}_k$. The lower bound is therefore obtained by convex minimization within the permitted fraction intervals. The upper bound occurs at an extreme point of the constrained polytope, where all but at most one fraction lie on one of their allowed boundaries.

The realistic bounds form a restricted subset of the tight bounds because $\mathcal{P}_k$ is itself a subset of the full stellar-population simplex. Consequently:

$$P_{\min}^{\text{tight}}\leq P_{\min}^{(k)}\leq P(\bar{\boldsymbol{\phi}})\leq P_{\max}^{(k)}\leq P_{\max}^{\text{tight}} \tag{48}$$

At $k=0$, the admissible domain reduces to the reference population and the lower and upper bounds coincide. Increasing k progressively enlarges the admissible population space. The default $k=3$ therefore allows each stellar fraction to vary by up to three adopted standard deviations around its reference value, subject at all times to non-negativity, the individual interval limits, and conservation of the total mass.

For the binding-energy equation derived in this work, $\alpha=\beta=1$. These bounds therefore quantify the range of normalized binding energy permitted by a specified stellar-population family rather than by arbitrary mathematically admissible mixtures.

6 Treatment of galactic gas and clumping

The preceding derivation applies directly to baryonic matter whose mass participates coherently in the same gravitational density distribution. In the weak-field regime, the gravitational contribution does not depend on whether this matter is stellar or gaseous when both components share the same smoothed density profile. Consequently, gas that follows the stellar distribution can be included in the same collective mass and contributes with the full $M^{5/3}$ scaling derived above.

The exponent $5/3$ therefore represents the maximum energetic efficiency of the gas in this construction. It corresponds to the limiting case in which the gas participates coherently in the same large-scale gravitational distribution as the stellar component. If instead part of the gas forms distinct clumps, these structures acquire their own binding-energy contributions rather than participating completely in the collective term. For gas divided into clumps of masses m_a with $\sum_a m_a = M_g$, convexity gives:

$$\sum_a m_a^{5/3} < \left(\sum_a m_a\right)^{5/3} = M_g^{5/3} \tag{49}$$

for any non-trivial fragmentation. The collective 5/3 contribution is therefore maximal when the gas behaves as a single component following the stellar distribution. Fragmentation reduces this efficiency because part of the gas is transferred from the collective contribution to the individual contributions of the clumps. Since gaseous structures also have much lower intrinsic densities than stellar objects, their separate terms are further reduced through the $\rho^{1/3}$ dependence of the binding-energy equation.

This departure from the maximally coherent case can be represented phenomenologically by an effective mass exponent $\gamma \leq 5/3$. The limit $\gamma = 5/3$ corresponds to gas following the stellar distribution without an additional clumping correction, while progressively smaller values represent an increasing fraction of the gas contributing through separate low-density structures. The exponent is therefore interpreted as an effective measure of the gravitational coherence of the gaseous component rather than as a modification of the fundamental 5/3 scaling derived for a fully coherent mass distribution.

In the empirical analysis, the normalized mass relation can consequently be written using an adjustable exponent γ as $M_{\mathrm{BE}}/M_{\mathrm{bar}}^{\gamma}$, with 5/3 representing the maximum-efficiency limit. A value below 5/3 indicates that the baryonic gas does not participate completely in the stellar-like collective contribution and that a larger fraction of its gravitational energy is associated with separate clumps.

This interpretation also leads to an evolutionary expectation. Young, gas-rich galaxies should remain closer to the 5/3 limit when a large diffuse gaseous component follows the global baryonic distribution. Older galaxies have consumed a larger fraction of their gas and the remaining material has had more time to settle into gravitationally bound and spatially distinct structures. They are therefore expected to require a stronger clumping correction and, within the present parametrization, a lower effective exponent than younger gas-rich systems.

7 Empirical validation with SPARC rotation curves

The first empirical validation uses the SPARC rotation-curve sample [19]. At each measured radius r, the baryonic mass $M_{\mathrm{bar},r}$ and the additional dynamical mass $M_{\mathrm{drk},r}$ required to reproduce the observed rotation velocity are evaluated as enclosed masses. The empirical hypothesis tested here is $M_{\mathrm{drk},r} = E_{p,r}/c^2$.

Rather than imposing the theoretically derived exponent 5/3, the mass exponent γ was allowed to vary independently over the very broad interval $[-5, 5]$. For every tested value of γ, each radial measurement was represented by $M_{\mathrm{drk},r}/M_{\mathrm{bar},r}^{\gamma}$ and compared with the binding-energy bounds derived above.

A radial point is considered compatible when it lies between the corresponding lower and upper bounds. A galaxy satisfies the test only when every measured radial point of that galaxy lies within the bounds for the same exponent. This galaxy-level criterion is therefore considerably more restrictive, since a single incompatible radius rejects the entire galaxy.

For the population-specific test, the admissible stellar-population bounds also depend on galactocentric radius. At radii $r \geq 10\,\mathrm{kpc}$, each point is compared with the specialized bounds associated with the morphological population of the galaxy. Inside $10\,\mathrm{kpc}$, a point is also considered compatible when it lies within the Kroupa bounds. This additional central criterion represents the more Kroupa-like stellar population expected in the inner regions of galaxies. A galaxy remains compatible only if every radial point satisfies the applicable criterion.

7.1 Localization of the mass exponent

The most striking result of the exponent scan is its strong localization. Although γ was explored over the full interval $[-5, 5]$, encompassing a range of ten exponent units, compatible solutions occur only within a narrow region close to the theoretically derived value $5/3 \simeq 1.667$. Outside this region, no radial point satisfies the bounds.

For the complete SPARC sample using the tight mathematical bounds, the first compatible point appears only at $\gamma = 1.45$ and the last at $\gamma = 1.83$. The galaxy-level criterion is still more restrictive, with compatible galaxies occurring only for $1.51 \leq \gamma \leq 1.76$. Everywhere else in the explored interval from -5 to 5, the number of compatible galaxies is exactly zero.

Table 5: Localization of compatible solutions within the exponent interval $\gamma \in [-5, 5]$. The intervals indicate the complete range over which at least one point or one entire galaxy satisfies the corresponding bounds.

Population bounds	Points non-zero	Galaxies non-zero	Best γ
Tight, all galaxies	1.45–1.83	1.51–1.76	1.62
Early	1.50–1.72	1.56–1.64	1.62
Intermediate	1.51–1.75	1.56–1.69	1.63
Late	1.56–1.76	1.58–1.70	1.66
Irregular	1.55–1.79	1.59–1.72	1.66

Thus, the empirical test did not merely select a favorable value from a narrow interval constructed around 5/3. Nearly the entire explored exponent domain produces no compatible solution at all. The admissible region emerges spontaneously from the SPARC data and remains centered close to the theoretical 5/3 scaling for both the unrestricted and population-specific bounds.

For the full sample, the concentration becomes particularly pronounced near the maximum:

Table 6: Compatibility of the complete SPARC sample with the tight mathematical bounds near the narrow region selected from the full interval $\gamma \in [-5, 5]$.

γ	Points	Points (%)	Galaxies	Galaxies (%)
−5.00–1.44	0	0.00	0	0.00
1.45	1/3256	0.03	0/175	0.00
1.50	362/3256	11.12	0/175	0.00
1.55	2707/3256	83.14	94/175	53.71
1.58	3232/3256	99.26	160/175	91.43
1.60	3248/3256	99.75	169/175	96.57
1.61	3253/3256	99.91	172/175	98.29
1.62	3255/3256	99.97	174/175	99.43
1.63	3251/3256	99.85	170/175	97.14
1.65	3230/3256	99.20	163/175	93.14
1.67	3049/3256	93.64	143/175	81.71
1.70	1766/3256	54.24	101/175	57.71
1.75	227/3256	6.97	5/175	2.86
1.76	118/3256	3.62	2/175	1.14
1.77	51/3256	1.57	0/175	0.00
1.83	3/3256	0.09	0/175	0.00
1.84–5.00	0	0.00	0	0.00

The transition is therefore not only localized but sharp. Starting from zero compatibility over most of the explored domain, the fraction of compatible galaxies rises to 99.43% at $\gamma = 1.62$ and then falls back to zero by $\gamma = 1.77$. The theoretical exponent $5/3 \simeq 1.667$ lies inside this narrow empirical region.

The population-specific results also support the gas-clumping interpretation introduced above. Late and Irregular galaxies reach their maximum compatibility at $\gamma = 1.66$, essentially indistinguishable from the theoretical maximum-efficiency value $5/3$. These younger, gas-rich systems therefore require little or no reduction of the collective gas contribution. Intermediate galaxies peak at $\gamma = 1.63$, indicating a moderate departure from the fully coherent limit, while Early galaxies peak at the still lower value $\gamma = 1.62$. The ordering is therefore exactly that expected if gravitational evolution progressively transfers part of the gaseous component from the large-scale collective distribution into more compact and individually bound structures. Older galaxies require the strongest effective clumping correction, intermediate galaxies require less, and the youngest populations remain closest to the unclumped $5/3$ limit.

The breadth of the exponent search also provides a simple estimate of how unlikely the observed localization would be under a uniform random placement within the explored interval. The exponent was scanned from -5 to 5 in steps of 0.01, corresponding to approximately one thousand possible tested values. For the full sample and the Intermediate population, the region surrounding the maximum spans eleven tested exponent values. The probability that the independently derived theoretical value $5/3 \simeq 1.66$ would fall inside such a narrow region by chance is therefore of order 11/1000, and hence below 1/90. For the Late and Irregular populations, the maximum occurs exactly at $\gamma = 1.66$. Under the same uniform-placement interpretation, the probability of an exact coincidence with one particular tested exponent is approximately 1/1000.

These estimates are not intended as formal statistical p-values, since neighboring exponent tests and galaxy populations are not independent. They quantify instead the geometric localization of the empirical solution within the deliberately broad interval explored. The fact that the independently predicted value lies inside the narrow admissible region in all cases, and coincides exactly with the maximum for both Late and Irregular galaxies, provides additional support for the predicted 5/3 scaling and for its gas-clumping interpretation.

7.2 Projection into the stellar-population space

The exponent scan constrains the mass scaling, but the normalization provides an independent test of the binding-energy prediction. Dividing the inferred missing mass by $M_{\mathrm{bar}}^{\gamma}$ removes the dominant dependence on the absolute baryonic mass and projects every radial measurement into the mass-independent stellar-population space derived above.

For the tight mathematical bounds, the complete admissible population space spans only about seven orders of magnitude. The specialized bounds associated with individual morphological populations are considerably narrower and span only about two orders of magnitude. Each SPARC radial measurement must therefore fall inside a restricted interval determined by the stellar-population model rather than by the mass scale of the galaxy.

At the best exponent for the complete sample, $\gamma = 1.62$, 3255 of the 3256 radial measurements, or 99.97%, lie inside the tight population bounds. Moreover, 174 of the 175 galaxies, or 99.43%, have every measured radial point inside these bounds. The latter criterion is particularly restrictive because a single radial measurement outside the predicted interval is sufficient to reject the entire galaxy.

It is therefore notable that galaxies covering widely different baryonic masses and radial distributions collapse into the same comparatively narrow population space after normalization. The agreement is not limited to reproducing an empirical mass slope. The normalization itself is constrained by the independently derived stellar-density bounds.

The best exponents obtained independently for the complete sample and for each morphological population are summarized in Table 7.

The agreement is therefore not limited to the recovery of a particular mass exponent. Once the mass dependence is removed, the SPARC measurements are also confined to the narrow normalization interval predicted from the stellar-population bounds. The simultaneous agreement in both exponent and normalization provides a substantially stronger test than either constraint considered independently.

To visualize how the observed galaxies populate the stellar-population space, we project them onto the same generic reference population used to define the plausible

Table 7: Best mass exponents obtained from the SPARC exponent scan. The complete sample uses the tight mathematical bounds, while the morphological classes use their corresponding specialized population bounds.

Sample	Best γ	Points inside	Points (%)	Galaxies inside	Galaxies (%)
All, tight	1.62	3255/3256	99.97	174/175	99.43
Early	1.62	876/938	93.39	14/28	50.00
Intermediate	1.63	949/1062	89.36	28/50	56.00
Late	1.66	773/783	98.72	47/53	88.68
Irregular	1.66	456/473	96.41	37/44	84.09

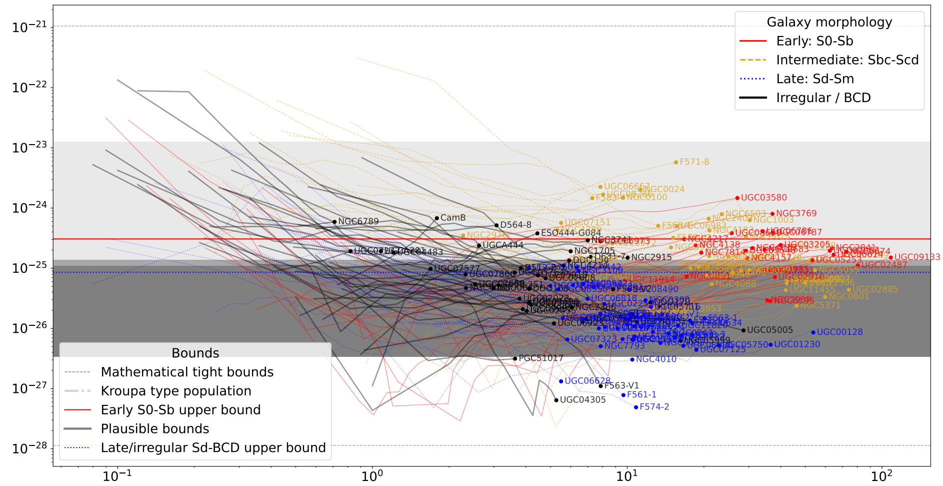

Fig. 1: Projection of the galaxies into the stellar-population space using the generic reference population associated with the plausible bounds listed in Table 3. For each morphological supertype, the plotted projection uses the mean exponent that maximizes the number of points entering the corresponding plausible corridor. Early and Intermediate galaxies favor exponents around 1.62, whereas Late and Irregular galaxies cluster very close to the theoretical value 5/3.

bounds shown in the graphical analysis and listed in Table 3. For each broad morphological family (Early, Intermediate, Late, and Irregular), we then determine the mean exponent that maximizes the number of projected points entering the corresponding plausible corridor. This provides a simple empirical way to place the galaxies on a common reference population while preserving the characteristic scaling preferred by each family.

The resulting projection is shown in Figure 1. The inferred average exponents are remarkably structured. Early-type galaxies prefer a mean exponent of 1.61789 (28 galaxies; standard deviation 0.00159), while Intermediate galaxies are only slightly higher, with a mean exponent of 1.62405 (50 galaxies; standard deviation 0.00277). In contrast, Late galaxies cluster very close to the theoretical value 5/3, with a mean exponent of 1.66652 (53 galaxies; standard deviation 3.42×10^{-4}), and Irregular galaxies behave similarly, with a mean exponent of 1.66547 (44 galaxies; standard deviation 0.00134). Thus, the projection naturally separates the sample into two broad regimes: Early and Intermediate systems favor slightly smaller exponents, whereas Late and Irregular systems lie extremely close to the 5/3 scaling.

What is particularly remarkable is that this organization emerges under very limited constraints. All galaxies are projected using the same generic stellar population and the same plausible bounds, with only the exponent adjusted independently for each morphological supertype. Despite this restricted construction, only seven galaxies fall outside the admissible region. Moreover, the distribution within this region is clearly structured: all Late galaxies lie below the Late/Irregular upper bound, while Early galaxies systematically occupy higher values, with most remaining below the Early upper bound and a subset extending into the Kroupa-compatible region. The Intermediate population follows the Early distribution closely, whereas the Irregular population is concentrated near the Late galaxies. Thus, the projection does not merely place most galaxies inside the allowed stellar-population space; it also recovers a coherent morphological ordering within that space from a remarkably small number of constraints.

The projection also provides a direct way to connect the dynamical reconstruction with independent photometric observations. The generic population should not be regarded as a single fixed stellar mixture, but as the reference point of a continuous family of populations. By varying its stellar fractions within their admissible ranges, the estimator can be continuously displaced across the plausible band. Consequently, for essentially any position reached by a galaxy within this band, a corresponding variation of the generic population can be constructed whose predicted dynamical value matches that position. The same procedure can also be continued beyond the nominal plausible bounds by allowing larger departures from the reference population, thereby extending the accessible stellar-population space.

This makes it possible to associate each galaxy with a stellar population selected solely from its dynamical position. That reconstructed population can then be used to predict independent photometric observables. We therefore compare the colors inferred from these dynamically selected populations with measurements from GALEX and SDSS [2, 20]. Unlike the dynamical matching itself, these photometric data do not enter the reconstruction and thus provide an independent test of whether the population variations required by the gravitational estimator correspond to real variations in the stellar content of galaxies.

8 Comparison with GALEX and SDSS Photometry

To associate each dynamical position with a stellar population, we introduce a simple multi-scale greedy reconstruction of the stellar fractions. Starting from the generic reference population of Table 3, the fractions are varied iteratively in order to reproduce the normalized mass inferred from the galaxy dynamics.

For a stellar population described by the fraction vector $\boldsymbol{\phi} = (\phi_1, \ldots, \phi_n)$, each trial population produces a predicted normalized mass $\mathcal{M}_{\rm pred}(\boldsymbol{\phi})$. The optimization minimizes the relative difference with the observed normalized mass:

$$\mathcal{E}_{\rm norm}(\boldsymbol{\phi}) = \frac{|\mathcal{M}_{\rm pred}(\boldsymbol{\phi}) - \mathcal{M}_{\rm obs}|}{\mathcal{M}_{\rm obs}} \tag{50}$$

At each iteration, the stellar fractions are perturbed locally around the current population, renormalized, and the modification producing the largest reduction of $\mathcal{E}_{\rm norm}$ is retained. The amplitude of the perturbations is progressively reduced until no further improvement is obtained. This procedure provides, for each galaxy, a stellar population whose gravitational estimator reproduces its position in normalized-mass space.

8.1 Dependence on the global binding-energy coefficient

We first evaluate the photometric reconstruction for the symmetric case $\alpha = \beta = 1$. We then repeat exactly the same comparison with $\alpha = 1$ and $\beta = 0.5$. The same galaxy samples are retained in both configurations for each color index, allowing the effect of the change in β to be examined directly.

Table 8 summarizes the Pearson and Spearman correlations between the predicted and observed GALEX/SDSS colors. For $\alpha = \beta = 1$, strong correlations are already recovered for $g - r$ and NUV–r, while $r - z$ shows a moderate correlation and FUV–NUV remains weak and negative. Reducing β to 0.5 preserves and generally strengthens the optical and UV–optical ordering, while producing a particularly large change in FUV–NUV.

Table 8: Correlation analysis between predicted and observed GALEX/SDSS colors for two values of the binding-energy coefficients.

	N	$r_{\rm P}$	$\sigma_{\rm P}$	$\rho_{\rm S}$	$\sigma_{\rm S}$
		$\alpha = 1,\ \beta = 1$			
FUV–NUV	136	-0.206	2.40	-0.202	2.35
$r - z$	129	0.336	3.90	0.403	4.73
$g - r$	128	0.598	7.45	0.574	7.09
NUV–r	119	0.603	7.26	0.593	7.11
		$\alpha = 1,\ \beta = 0.5$			
FUV–NUV	136	0.403	4.87	0.459	5.62
$r - z$	129	0.264	3.02	0.413	4.87
$g - r$	128	0.623	7.86	0.619	7.78
NUV–r	119	0.634	7.75	0.631	7.70

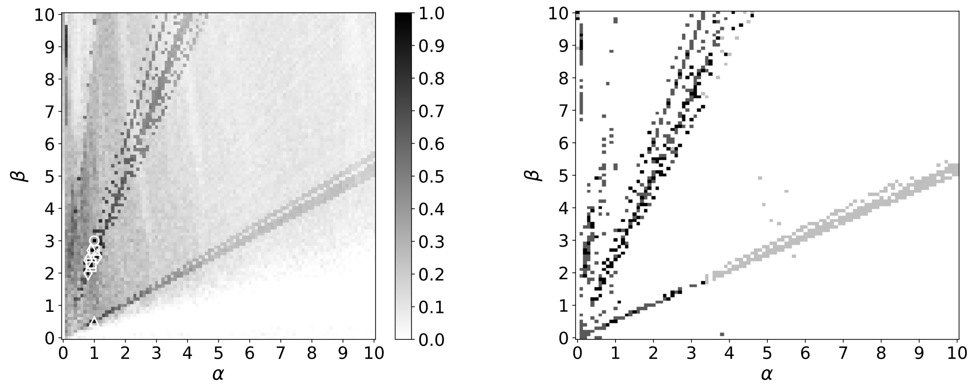

(a) Normalized photometric score over the (α, β) grid. Darker shades correspond to higher scores, while the white symbols identify the nine highest-scoring solutions.

(b) Preferred regions of parameter space. Light gray marks the five best values of β for each fixed α, dark gray marks the five best values of α for each fixed β, and black marks solutions selected by both criteria.

Fig. 2: Photometric exploration of the two-term binding-energy estimator. The preferred solutions are strongly concentrated around $\alpha = 1$, while the dependence on β remains broader and extends on both sides of $\beta = 1$.

8.2 Photometric exploration of the estimator

The binding-energy estimator introduced in Equations (30) and (34) contains two coefficients with distinct roles. The coefficient α controls the contribution associated with the homogeneous stellar classes, while β controls the global aggregation contribution.For each pair (α, β), stellar populations are generated from the normalized-mass constraint and their predicted GALEX and SDSS colors are compared with the observations. The Pearson and Spearman significances obtained for FUV–NUV, NUV–r, $g - r$, and $r - z$ are combined into a single photometric score. The resulting score therefore provides an independent test of the stellar populations generated by different values of the two coefficients.

Figure 2 shows the exploration of the (α, β) parameter space. In panel (a), the gray scale represents the normalized photometric score over the complete grid, with darker regions corresponding to higher scores. The white symbols identify the nine highest-scoring configurations. Panel (b) emphasizes the location of the preferred solutions independently of their absolute score. For each fixed α, the five best values of β are shown in light gray. For each fixed β, the five best values of α are shown in dark gray. Points selected by both criteria are shown in black.

The most prominent feature in both representations is the concentration of the preferred solutions around $\alpha = 1$. The highest-scoring configurations lie close to this value, and the selected regions become progressively less concentrated as α moves away from unity. The dependence on β is broader. High-quality solutions occur both below and above $\beta = 1$, while remaining concentrated around values of order unity. This weaker constraint is consistent with the smaller contribution of the global term, which represents only approximately 10% of the total binding energy.

The concentration around $\alpha = 1$ is particularly significant because this value is independently obtained from the hierarchical construction of the estimator, in which the binding energies already stored in the stellar classes are retained with unit weight. The agreement between this theoretical value and the photometrically preferred region is therefore unlikely to be accidental. The broader range of preferred β values is also consistent with its smaller influence on the total energy. Importantly, changing α from 1 to 0.5 does not produce any significant visible change in the position or width of the admissible bands. What changes is the distribution of the stellar populations generated within those bands.

The photometric comparison therefore constrains the stellar populations generated within the admissible bands, rather than the position or width of the bands themselves. The coincidence with the theoretically expected coefficients is also non-trivial from a simple probabilistic point of view. If no value of α were preferred and the 100 sampled α positions were equally likely to contain the optimum, the probability for the preferred value to coincide with the independently predicted value $\alpha = 1$ would be of order $1/100$. In the full two-dimensional exploration, containing approximately 10^4 sampled (α, β) positions, the coincidence of the preferred region with the theoretically motivated location $\alpha = 1$ and β of order unity is correspondingly much more restrictive. For a single pre-specified grid position, the naive combinatorial probability would be of order 10^{-3}, increasing only in proportion to the width assigned a priori to the acceptable neighborhood around $\beta = 1$.

These estimates should not be interpreted as formal statistical p-values because neighboring grid points are correlated and the photometric score varies continuously across parameter space. They nevertheless provide a useful measure of how non-trivial the observed agreement is. The value $\alpha = 1$ and a global coefficient β of order unity are obtained independently from the physical construction of the estimator. Their recovery from the photometric exploration therefore constitutes an important validation of the proposed binding-energy form.

8.3 Statistical robustness of the population-space relation

The correlations reported in Table 8 indicate that the positions assigned to the galaxies in stellar-population space are related to their independently observed photometric properties. Since the GALEX and SDSS colors are not used to determine these positions, the comparison provides an a posteriori test of the projection. We now examine whether these correlations could instead result from finite-sample fluctuations or from the distribution of inclination and morphology in the sample.

The analysis is performed independently for $(\alpha, \beta) = (1, 1)$ and $(1, 1/2)$. Since the quantity of interest is primarily the ordering of the galaxies in population space, Spearman's rank coefficient is used as the main statistic. Pearson correlations lead to the

Table 9: Robustness of the relation between predicted and observed photometric ordering. The bootstrap interval gives the 16th and 84th percentiles of the Spearman coefficient. Flip is the fraction of bootstrap realizations in which its sign changes, JK SE is the jackknife standard error, and $\sigma_{\rm perm}$ is the Gaussian-equivalent significance obtained from the permutation test.

Color	ρ_S	Bootstrap 16–84%	Flip	JK SE	$\sigma_{\rm perm}$
		$\alpha = 1,\ \beta = 1$			
FUV–NUV	-0.200	[-0.282,-0.114]	0.0102	0.085	2.32
$r - z$	0.401	[0.326, 0.470]	10^{-6}	0.073	4.65
$g - r$	0.581	[0.516, 0.638]	0	0.062	5.73
NUV–r	0.601	[0.530, 0.665]	0	0.069	5.73
		$\alpha = 1,\ \beta = 1/2$			
FUV–NUV	0.454	[0.379,0.522]	0	0.072	5.49
$r - z$	0.402	[0.325,0.473]	3×10^{-6}	0.075	4.66
$g - r$	0.629	[0.568,0.682]	0	0.058	5.73
NUV–r	0.646	[0.582,0.702]	0	0.061	5.73

same general conclusions and are not repeated here. For each configuration, 10^6 bootstrap realizations, leave-one-out jackknife estimates, and 10^8 random permutations are evaluated.

The optical and UV–optical relations are remarkably stable between the two energy prescriptions. For $r - z$, $g - r$, and NUV–r, the bootstrap intervals remain entirely on the same side of zero, sign reversals are absent or extremely rare, and the jackknife uncertainties remain small. The permutation tests independently reject random galaxy–color associations at 4.65σ for $r - z$ and at the 10^{-8} numerical sampling limit, corresponding to approximately 5.73σ, for both $g - r$ and NUV–r. The purely ultraviolet FUV–NUV color is the main exception. It shows a weaker anticorrelation for $\beta = 1$, significant at 2.32σ, but a positive correlation reaching 5.49σ for $\beta = 1/2$. The sensitivity of this color to β contrasts with the stability of the three longer-wavelength indices.

The sample was also divided into low, intermediate, and high inclination ranges. The correlations are generally weak in the low-inclination subsamples, which are also the smallest, but reappear strongly at intermediate and high inclinations. Across the two values of β, the Spearman permutation significances in these two inclination ranges reach 4.43–5.73σ for $g-r$ and 4.83–5.73σ for NUV–r. The $r-z$ relation remains detectable with significances from 2.71 to 4.69σ. FUV–NUV again shows the strongest dependence on the adopted value of β. The persistence of the optical and UV–optical ordering after subdivision by inclination indicates that the global relation cannot be explained simply by mixing galaxies observed at different viewing angles.

A complementary test is obtained by separating early-type spirals (S0–Sb), late-type spirals (Sbc–Sdm), and irregular systems (Sm–BCD). The strongest internal ordering is consistently found among late-type spirals. For $\beta = 1$ and $1/2$, respectively, the Spearman permutation significance is 2.58σ and 2.60σ for $r - z$, 4.26σ and 3.93σ for $g - r$, and 3.80σ and 3.23σ for NUV$-r$. The early-type and irregular subsamples show substantially weaker relations. The survival of the correlation within a single broad morphological class is important because it shows that the global ordering is not produced solely by placing different morphological families at different locations in population space.

The mass-ranking tests show that baryonic and dynamically inferred dark masses are very strongly correlated in the SPARC sample, with Spearman coefficients close to 0.95. The observed and reconstructed optical rankings also retain a strong dependence on the global mass scale. This behavior is precisely what is expected from the binding-energy equation, in which the dominant mass dependence factorizes from the stellar-population contribution and is explicitly removed by the normalization. The mass-ranking results therefore provide an additional experimental validation of this structure of the equation.

Taken together, the bootstrap, jackknife, permutation, inclination, and morphology tests strongly disfavor an interpretation in which the population-space relation is produced by a few individual galaxies, random associations, viewing geometry, or the simple separation of morphological classes. The recovery of essentially the same optical and UV–optical ordering for both $\beta = 1$ and $\beta = 1/2$ further shows that this result is not fine-tuned to a single value of the global energy coefficient. The correspondence between the dynamical projection and independent photometry therefore provides direct evidence that the positions occupied by the galaxies in stellar-population space contain physically meaningful information.

9 Dark mass and dark energy

The results obtained at galactic scales motivate a more speculative extension of the present framework. If the effective dark mass inferred from dynamics represents gravitational binding energy, the same hierarchical construction should not necessarily terminate at the scale of individual galaxies. Galaxies themselves may be regarded as bound subsystems that can contribute to the gravitational energy of larger structures. This extension is nevertheless limited by cosmic expansion, and therefore requires a transition from the local weak-field treatment used above to a cosmological description.

9.1 Extragalactic extension and the turnaround scale

At galactic scales, characteristic velocities are small and cosmic expansion does not significantly affect the internal dynamics, so that the Newtonian weak-field approximation remains adequate. At sufficiently large distances, however, expansion eventually competes with gravitational binding. A natural boundary is provided by the turnaround radius of a bound structure. In a Schwarzschild–de Sitter description, its maximum value is:

$$R_{\mathrm{ta,max}} = \left(\frac{3GM}{\Lambda c^2}\right)^{1/3} \tag{51}$$

which defines the largest scale on which a mass M can remain gravitationally bound in the presence of a positive cosmological constant [22, 26].

This provides a natural hierarchical continuation of the construction developed in this work. Stellar classes are first combined into galaxies, and galaxies can then be combined within gravitationally bound turnaround regions. In an initial simple implementation of this idea, turnaround cells containing from a few galaxies to several hundred were sufficient to generate an extragalactic binding-energy contribution of the same order as the cosmological dark-mass component. The required cell populations were comparable to those expected for isolated systems, groups, and clusters. This result should not be interpreted as an independent cosmological determination, but it suggests that the hierarchical energy construction can remain physically meaningful beyond the scale of individual galaxies.

The turnaround condition is particularly important because it prevents the gravitational-energy calculation from being extended arbitrarily over the entire Universe. Interactions between systems separated beyond their effective gravitational domain should not be treated in the same way as interactions within a bound structure. The turnaround scale therefore marks the approximate transition between locally generated binding energy and the large-scale gravitational field associated with cosmic expansion.

An important consequence appears when the same construction is extended to earlier epochs. Two effects then act simultaneously. First, the stellar populations evolve with redshift. The smaller fraction of dense stellar remnants at early times lowers the characteristic stellar density and therefore reduces the galactic binding-energy contribution. Second, the turnaround scale itself evolves. At higher redshift, the effective turnaround radius becomes smaller, reducing the size and mass of the regions within which galaxies can remain gravitationally bound. The extragalactic binding-energy contribution therefore decreases even more rapidly. As a result, although the gravitational-energy mechanism reproduces the expected dark-mass scale at $z = 0$, the agreement progressively disappears toward higher redshift. The predicted galactic contribution falls to about 41% of its expected value at $z = 5$ and 11% at $z = 10$, while the extragalactic contribution falls to about 10% and 2%, respectively.

This produces what we call a cosmological hypercoincidence. Two independent physical evolutions, the changing stellar density and the changing turnaround scale, both drive the predicted dark mass away from its present-day value. The success at $z = 0$ therefore appears as a very specific epoch rather than a generic consequence of the model. This empirical constraint is what motivates the possible exchange between gravitational and vacuum energy developed below.

9.2 Gravitational–vacuum energy exchange

A deeper connection follows by allowing gravitational binding energy to exchange energy with the vacuum. General relativity guarantees local covariant conservation, while an expanding spacetime does not in general admit a globally conserved energy associated with time-translation symmetry. The key step is to allow the effective cosmological term to vary locally in spacetime, $\Lambda = \Lambda(x^\mu)$, rather than treating it as a fixed universal constant. This avoids imposing a separate global conservation law on the gravitational sector, which would encounter the usual Noether limitation. Local changes in gravitational energy can then be compensated by corresponding changes in the vacuum contribution, while the combined stress–energy remains covariantly conserved.

At the covariant level, this can be written as:

$$\nabla_\mu T^{\mu\nu} = -\frac{c^4}{8\pi G}\nabla^\nu \Lambda \qquad \Longleftrightarrow \qquad \nabla_\mu \left(T^{\mu\nu} + T^{\mu\nu}_{(\Lambda)}\right) = 0 \tag{52}$$

For a gravitationally bound turnaround cell followed through cosmic evolution, let $V_{\rm ta}(t)$ denote its physical volume and define:

$$\Theta_{\rm ta} = \frac{\dot{V}_{\rm ta}}{V_{\rm ta}}$$

The exchange between gravitationally stored energy and the vacuum sector may then be written as:

$$\dot{\rho}_{\rm grav} + \Theta_{\rm ta}\rho_{\rm grav} = Q, \qquad \dot{\rho}_\Lambda + \Theta_{\rm ta}\rho_\Lambda = -Q \tag{53}$$

where Q represents the energy transferred between the two sectors within the same turnaround cell.

Equivalently, defining $E_{\rm grav} = \rho_{\rm grav} V_{\rm ta}$ and $E_\Lambda = \rho_\Lambda V_{\rm ta}$ gives:

$$\frac{d}{dt}\left(E_{\rm grav} + E_\Lambda\right) = 0 \tag{54}$$

Under this interpretation, dark mass and dark energy are no longer independent components. Dark mass represents gravitational energy stored in bound structures, while the vacuum sector provides the complementary cosmological contribution required as this energy changes during structure formation and cosmic expansion.

This possibility is especially relevant because the galactic contribution to gravitational energy is not expected to remain constant with redshift. As stellar populations evolve, the amount of binding energy stored at galactic scales changes. A compensating vacuum term would allow the global gravitational energy budget to remain conserved across the ensemble of evolving turnaround cells, even though its partition between bound structures and the cosmological background evolves.

The turnaround scale naturally enters this exchange. It separates gravitationally bound regions, within which potential energy can be stored as an effective dark mass, from the expanding background, within which the vacuum contribution dominates the large-scale evolution. Changes in the characteristic turnaround scale therefore provide a possible physical interface between the two sectors.

9.3 Thermodynamic closure and a zero-energy Universe

The exchange described above suggests a broader interpretation of the cosmological energy budget. General relativity does not require a globally conserved energy in a generic expanding spacetime, whereas the first law of thermodynamics expresses conservation of energy for a closed system. These statements are not mathematically contradictory, since they apply within different conceptual frameworks. The present hypothesis nevertheless provides a possible way of making them compatible at the scale of the Universe as a whole.

If dark mass is gravitational potential energy, the positive energy content of the Universe contains not only baryonic rest energy but also the gravitational energy stored through the formation of bound structures. We may therefore write:

$$E_+ = E_{\mathrm{b}} + E_{\mathrm{pot}}. \tag{55}$$

The thermodynamic closure proposed here assigns the cosmological vacuum sector the compensating contribution:

$$E_{\mathrm{tot}} = E_{\mathrm{b}} + E_{\mathrm{pot}} + E_{\Lambda}. \tag{56}$$

The strongest form of the hypothesis is then:

$$E_{\mathrm{tot}} = 0, \qquad E_{\Lambda} = -\left(E_{\mathrm{b}} + E_{\mathrm{pot}}\right). \tag{57}$$

Other contributions, such as radiation, may be included in the global energy balance without altering the conservation principle developed here; they are omitted for clarity because they do not affect the gravitational–vacuum mechanism considered in this work.

In this picture, all positive energy associated with baryonic matter and gravitational potential energy is exactly compensated by the cosmological contribution. The total energy of the Universe is therefore zero, while its observable contents correspond to different redistributions of this vanishing global balance.

The significance of this interpretation extends beyond the dark-sector problem. General relativity provides a local geometrical description of gravitation and guarantees covariant conservation, but does not generally define a conserved global energy for an expanding Universe. Thermodynamics, by contrast, motivates conservation of the total energy of a closed system. The extended conservation proposed above provides a possible bridge between these two descriptions. Local evolution remains governed by general relativity, while the global energy budget is constrained by thermodynamic conservation.

Dark mass and dark energy then acquire complementary roles within the same conservation principle. The formation of gravitational structure increases the positive potential-energy contribution stored in bound systems. The vacuum sector changes correspondingly so that the total balance remains unchanged. Cosmic evolution becomes an exchange between two sectors rather than the creation or destruction of net energy.

The condition $E_{\text{tot}} = 0$ gives this construction an especially simple interpretation. The Universe can contain enormous positive amounts of baryonic and gravitational energy without requiring a non-zero net energy content. The corresponding cosmological contribution balances these terms exactly. Structure formation, gravitational binding, and accelerated expansion can then be interpreted as different manifestations of a single globally conserved energy budget.

This also changes the interpretation of the cosmological coincidence problem. Dark mass and dark energy need not have comparable magnitudes by accident if they are linked by the same conservation condition. Their relative values become consequences of how the total energy is partitioned between gravitationally bound structures and the cosmological background at a given epoch.

The zero-energy condition remains an additional physical hypothesis and is not a consequence of the Einstein equations alone. Its interest lies in the possibility that the apparent absence of global energy conservation in cosmological general relativity does not reflect a failure of thermodynamics, but rather the absence of a complete accounting of gravitational and vacuum contributions. If this interpretation is correct, the dark sector would represent the mechanism through which general relativity and the first law of thermodynamics become compatible at the scale of the Universe.

10 Discussion

The central question addressed in this work is remarkably simple. If all the stars of a galaxy underwent an idealized perfectly inelastic aggregation, while only gravitational interactions were considered, how much energy would be released? The quantity calculated here is intended to represent precisely this energy. It is the gravitational energy stored in the internal organization of the galaxy and potentially available for release through a change of configuration.

The connection with dark mass follows only after this energy has been identified. Through mass–energy equivalence, a physically stored gravitational energy corresponds to an effective mass contribution. If this contribution participates in the gravitational field of the system, it must also affect the curvature of spacetime and the motion of test bodies. The observational question is therefore whether the gravitational effects conventionally attributed to an additional dark matter component can instead correspond to the mass equivalent of this binding energy.

For decades, the simplest interpretation of the missing-mass problem was to postulate an additional unseen matter component while preserving the known laws of gravitation. This interpretation was initially economical because the unknown component could plausibly be regarded as ordinary matter not yet observed, or as a new elementary-particle species. However, the progressive exclusion of dominant baryonic candidates and the continuing absence of an independently identified non-baryonic component substantially weaken this original argument from simplicity.

The interpretation proposed here restores that principle of economy in a different way. It requires neither a new form of matter nor a modification of the known laws of gravitation. The additional gravitating contribution arises from gravitational potential energy already present in the system together with standard mass–energy equivalence. The missing-mass problem is therefore recast not as evidence for an additional substance, but as a possible consequence of how gravitational energy is accounted for in bound systems.

The unusually broad domain over which the construction can be established provides an additional reason to consider this interpretation seriously. The Newtonian derivation remains valid over nearly forty orders of magnitude in mass while preserving the same functional form. Its breakdown at sufficiently high compactness reflects the breakdown of the Newtonian description itself, rather than a failure of the resulting mathematical structure. Moreover, an independent construction based on sequential relativistic absorption reaches the same expression without extending a hypothetical Newtonian configuration below its domain of validity. The convergence of these two physically distinct constructions strongly supports the robustness of the resulting relation.

A fully relativistic derivation would nevertheless remain theoretically valuable, particularly for clarifying the exact spacetime interpretation of the gravitational-energy contribution. It should not, however, be expected to provide a stronger validation of the equation itself. The relation is already supported independently by its persistence across nearly forty orders of magnitude, by the convergence of two distinct derivations, and by its observational agreement with galactic dynamics. A covariant derivation would therefore strengthen the theoretical foundation and interpretation of the result rather than its empirical validity.

Because each stellar-class contribution to the binding energy scales as M_i^2/R_i, with $R_i \propto (M_i/\rho_i)^{1/3}$, the total binding energy separates into a global baryonic-mass dependence proportional to $M^{5/3}$ and a normalization determined by the stellar-population fractions and intrinsic densities.

The predicted $M^{5/3}$ scaling was tested by temporarily replacing the exponent $5/3$ with a free exponent γ. For each value of γ, the observed dark-mass estimates were rescaled and compared with the theoretical bounds generated from the admissible stellar populations. The preferred exponent is therefore the one that places the largest number of radial measurements, and ultimately the largest number of complete galaxies, inside these independently defined bounds. This procedure produces a narrow optimum close to the predicted value $5/3$, with Late and Irregular galaxies lying closest to it.

The same comparison also tests the normalization of the equation. Once the mass dependence is removed, the remaining coefficient must fall within the range permitted by the stellar densities and population fractions entering the binding-energy expression. The populations reconstructed from these dynamical positions were then subjected to an independent test. No photometric information enters the reconstruction, yet their ordering correlates significantly with GALEX and SDSS colors.

The existence of known relations between galaxy mass, luminosity, and photometric properties does not weaken this test. The purpose of the reconstruction is not to introduce a new method for predicting galaxy colors, but to test whether stellar populations inferred solely through the binding-energy equation remain consistent with independently observed properties of the same galaxies. In this sense, the photometric correlations provide an experimental validation of the physical information recovered by the equation. Conversely, the relation identified here may offer a simple physical origin for at least part of the known connection between galactic mass and photometric properties.

Allowing the structural coefficients themselves to vary provides a further test of the derivation. The preferred solutions concentrate around the predicted class-level coefficient $\alpha = 1$, whereas the smaller global contribution governed by β remains less tightly constrained.

The experimental validation can now be extended beyond galactic rotation curves and stellar photometry. The same relation should be confronted with independent observables that probe the gravitational field in different ways, including gravitational lensing, stellar and gas dynamics outside galactic disks, satellite motions, galaxy groups, and clusters. Agreement across these independent regimes would test whether the same gravitational-energy contribution consistently accounts for the effects presently attributed to dark mass, rather than reproducing only one class of galactic observables.

Extending the construction to cosmological scales exposes a strong redshift dependence that is not resolved by the galactic mechanism alone. A possible exchange between gravitational and vacuum energy provides one route toward a unified interpretation of the dark sector, while the zero-energy condition represents a further thermodynamic hypothesis. These extensions remain speculative and provide additional opportunities for falsification.

The galactic results nevertheless show that gravitational binding energy possesses the predicted mass dependence, normalization, and stellar-population structure required to make its possible relation to dark mass directly testable.

11 Conclusion

This work proposes that the mass conventionally identified as dark mass can be interpreted as the mass equivalent of gravitational potential energy stored in bound structures. The derived relation follows from standard gravitational physics and mass–energy equivalence, without introducing an additional form of matter or modifying the known laws of gravitation. Its agreement with galactic observations indicates that this interpretation can account simultaneously for the magnitude and the structural dependence of the missing-mass phenomenon.

The present results establish a framework that can now be tested beyond the observables considered here. Extending these tests to gravitational lensing, external galactic dynamics, groups, clusters, and cosmological evolution will determine how broadly the same interpretation can account for phenomena presently attributed to dark matter. If this correspondence persists across these independent regimes, dark mass may be understood not as an additional substance, but as a manifestation of gravitational energy already contained in the structure of the Universe.

Software Availability

The C++ program used to perform all numerical calculations and generate the corresponding graphs are freely available at dark-mass-generator.sourceforge.io or at https://doi.org/10.6084/m9.figshare.33894055.

Declarations

Funding — This research received no specific grant from any funding agency in the public, commercial, or not-for-profit sectors.

Competing interests — The author declares no competing interests.

Ethics approval / Consent — Not applicable.

Data and materials availability — See “Software availability”.

Author contribution – N.P. conceived the study, performed the analysis, and wrote the manuscript.

References

[1] Bartelmann M (2010) Gravitational lensing. Classical and Quantum Gravity 27(23):233001. https://doi.org/10.1088/0264-9381/27/23/233001

[2] Bianchi L, et al (2011) Galex gr5 x sdss dr7 matched catalogs. MAST / STScI High-Level Science Products, uV and UV-optical matched source catalogs

[3] Blanton MR, Moustakas J (2009) Physical properties and environments of nearby galaxies. Annual Review of Astronomy and Astrophysics 47:159–210. https://doi.org/10.1146/annurev-astro-082708-101734

[4] Brillouin L (1965) The mass of a system of potential energy. Proceedings of the National Academy of Sciences of the United States of America 53(3)

[5] Bruzual G, Charlot S (2003) Stellar population synthesis at the resolution of 2003. Monthly Notices of the Royal Astronomical Society 344(4):1000–1028. https://doi.org/10.1046/j.1365-8711.2003.06897.x

[6] Clowe D, Bradač M, Gonzalez AH, et al (2006) A direct empirical proof of the existence of dark matter. The Astrophysical Journal Letters 648:L109–L113

[7] Courteau S, et al (2014) Galaxy masses. Reviews of Modern Physics 86:47–119

[8] Deur A (2021) Relativistic corrections to the rotation curves of disk galaxies. European Physical Journal C 81:213

[9] Deur A, Sargent C, Terzic B (2020) Significance of gravitational nonlinearities on the dynamics of disk galaxies. The Astrophysical Journal 896:94

[10] Eker Z, Bakis V, Bilir S, et al (2018) Interrelated main-sequence mass–luminosity, mass–radius, and mass–effective temperature relations. Monthly Notices of the Royal Astronomical Society 479(4):5491–5511. https://doi.org/10.1093/mnras/sty1834

[11] Fontaine G, Brassard P, Bergeron P (2001) The potential of white dwarf cosmochronology. Publications of the Astronomical Society of the Pacific 113(782):409–435. https://doi.org/10.1086/319535

[12] Gallazzi A, Charlot S, Brinchmann J, et al (2005) The ages and metallicities of galaxies in the local universe. Monthly Notices of the Royal Astronomical Society 362(1):41–58. https://doi.org/10.1111/j.1365-2966.2005.09321.x

[13] Hawking SW (1968) Gravitational radiation in an expanding universe. Journal of Mathematical Physics 9(4):598–604

[14] Hayward SA (1994) Quasilocal gravitational energy. Physical Review D 49(2):831–839. https://doi.org/10.1103/PhysRevD.49.831

[15] Hayward SA (1996) Gravitational energy in spherical symmetry. Physical Review D 53:1938–1949

[16] Kennicutt RC (1998) Star formation in galaxies along the hubble sequence. Annual Review of Astronomy and Astrophysics 36:189–232

[17] Kroupa P (2001) On the variation of the initial mass function. Monthly Notices of the Royal Astronomical Society 322(2):231–246. https://doi.org/10.1046/j.1365-8711.2001.04022.x

[18] Lattimer JM, Prakash M (2007) Neutron star observations: Prognosis for equation of state constraints. Physics Reports 442(1-6):109–165. https://doi.org/10.1016/j.physrep.2007.02.003

[19] Lelli F, McGaugh SS, Schombert JM (2016) Sparc: Mass models for 175 disk galaxies with spitzer photometry and accurate rotation curves. The Astronomical Journal 152(6):157

[20] Martin DC, et al (2005) The galaxy evolution explorer: A space ultraviolet survey mission. The Astrophysical Journal Letters 619:L1–L6

[21] Misner CW, Sharp DH (1964) Relativistic equations for adiabatic, spherically symmetric gravitational collapse. Physical Review 136:B571–B576

[22] Pavlidou V, Tomaras TN (2014) Where the world stands still: turnaround as a strong test of ΛCDM cosmology. Journal of Cosmology and Astroparticle Physics 2014(09):020

[23] Persic M, Salucci P, Stel F (1996) The universal rotation curve of spiral galaxies. Monthly Notices of the Royal Astronomical Society 281:27–47

[24] Rubin VC, Ford JW. Kent, Thonnard N (1980) Rotational properties of 21 sc galaxies with a large range of luminosities and radii, from ngc 4605 (r = 4kpc) to ugc 2885 (r = 122kpc). The Astrophysical Journal 238:471–487

[25] Szabados LB (2009) Quasi-local energy-momentum and angular momentum in general relativity. Living Reviews in Relativity 12(4):4. https://doi.org/10.12942/lrr-2009-4

[26] Tanoglidis D, Nesseris S, Pavlidou V (2015) Testing ΛCDM cosmology at turnaround: where to look for violations of the bound? Journal of Cosmology and Astroparticle Physics 2015(12):060

[27] Torres G, Andersen J, Gimenez A (2010) Accurate masses and radii of normal stars: modern results and applications. The Astronomy and Astrophysics Review 18(1-2):67–126. https://doi.org/10.1007/s00159-009-0025-1